Indian Journal of Biochemistry & Biophysics
Vol. 63, January 2026, pp. 40-62
DOI: 10.56042/ijbb.v63i1.18253

Potential bioactive ligand and its divalent M (II) complexes: Synthesis, physicochemical characterization, DFT calculations and biological applications

Ankit Kumar Choubey*, and AP Mishra

Department of Chemistry, Dr. Hari Singh Gour Vishwavidyalaya (A Central University), Sagar-470 003, Madhya Pradesh, India

Received 25 March 2025; *revised 19 June 2025*

A new series of Zinc, Copper, Nickel and Cobalt coordinated metal complexes have been harvested by newly synthesized bioactive ligand 2-chloro-6- ((2,5-dimethoxybenzylidene)amino)-4-nitrophenol (L) derived from 2,5-dimethoxybenzaldehyde and 2-Amino-6-chloro-4-nitrophenol. Synthesized compounds have been spectrochemically characterized by UV-visible, FT-IR, NMR, ESI-MS, Powder-XRD, elemental analysis, molar conductance, and cyclic voltammetry (CV). The chelation of metal ions to bioactive ligand L was confirmed by FT-IR data. Thermogravimetric analysis (TGA) has been used to investigate the thermal stability of synthesized complexes as well as to identify the coordinated and lattice water molecules. Non-electrolytic behavior of synthesized metal complexes was examined by study of molar conductance. Theoretical study has been carried out using the method DFT/B3LYP at basic sets 6-31G for the bioactive ligand L and LANL2DZ for the metal complexes (CoL, NiL, CuL, ZnL) respectively. Molecular Electrostatic Potential (MEP), Mulliken charges, HOMO-LUMO and global reactivity descriptors; chemical hardness (η), chemical potential (μ), global softness (S) and electrophilicity index (ω) have been estimated and correlated with antimicrobial activity. Biological evaluations of synthesized compounds exhibited potent antifungal activity against *Fusarium oxysporum* and *Aspergillus niger,* and antibacterial against *Staphylococcus aureus* and *E. coli.* All the synthesized compounds have also been screened for dye-degradation against methylene blue dye, in which Cu metal complex displayed better activity comparison to others.

Keywords: Antibacterial, Antifungal, Bioactive ligand and its metal chelates, DFT, Dye degradation, Spectroscopic characterization

The term 'Schiff base' was first used in 1864 by the great scientist Hugo Schiff, who prepared it during a condensation reaction between a carbonyl compound (ketone or aldehyde) and a primary amine[1]. The complexation ability of metal ions in existence of multidentate Schiff base ligands has been systematically deliberated in the area of coordination chemistry over the last few decades. They provide excellent binding opportunities by electrophilic carbon atom and nucleophilic nitrogen atom in -C=N- (imine) bond with different nucleophiles and electrophiles. Schiff base ligands and its coordinated transition metal complexes have gained enough attention due to their vast applications in multiple scientific platforms. Schiff bases, known for their sensitivity, versatility, and selectivity towards metal ions, are advantageous ligands with multifaceted applications across science and technology[2-4]. Their ability to form stable complexes with transition metals, attributed to the strength and steric competence of the azomethine group, makes them valuable in diverse fields. Consequently, they are explored for electroluminescence, fluorescence, and a wide range of biomedical applications, including antibacterial, antiviral, anticancer, antifungal[5-7], antituberculosis, DNA cleavage, DNA binding, analgesic, and antioxidant properties. Furthermore, due to their extensive chelating potential and facile synthesis, Schiff bases and their metal complexes find effective use in various disciplines, particularly as cost-effective and thermally stable oxidation catalysts for alcohols and alkenes[8-10]. Notably, they also hold promise in bio-medicinal applications, such as DNA photocleavage. 2-Amino-6-chloro-4-nitrophenol is a valuable intermediate in the synthesis of dyes and pigments due to its ability to participate in various chemical reactions. This compound is also utilized in materials science for the development of colorants and the production of compounds with applications in electronics and photonics. Furthermore, it holds

*Correspondence:
Phone: +91-8109558033 (Mob)
E-mail: ankit.choubey94@gmail.com
Suppl. data available on respective page of NOPR

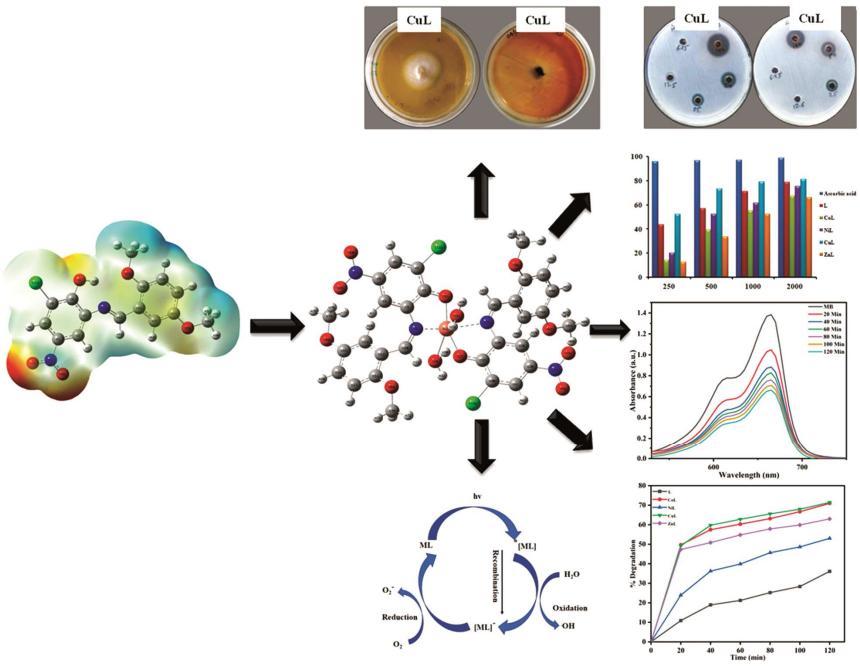

Graphical abstract

potential for the development of colorimetric sensors capable of detecting specific analytes through color changes[11].

The significance of this study is threefold. First, it introduces a novel Schiff base ligand, 2-chloro-6-((2,5-dimethoxybenzylidene)amino)-4-nitrophenol, with a unique combination of electron-donating and electron-withdrawing groups that enhance its coordination ability and structural diversity. Second, the synthesized ligand and its metal (II) complexes with Zn, Cu, Ni, and Co have been evaluated for their antimicrobial activity, providing potential leads for new antibacterial and antifungal agents. Third, the metal complexes were tested for their photocatalytic performance in dye degradation, demonstrating their practical applicability in environmental remediation and industrial catalysis. Together, these aspects highlight the ligand's multifunctionality and its relevance in both bioinorganic and materials chemistry.

The literature suggests that there are several gaps in research on the novel bioactive ligand 2-chloro-6-((2,5-dimethoxybenzylidene)amino)-4-nitrophenol (L) and its metal complexes with Zinc, Copper, Nickel, and Cobalt metal (II), particularly in the areas of structural features and applications. The coordination behavior of the potential ligand L and its metal chelates (CoL, NiL, CuL, ZnL) has been investigated through spectrochemical, analytical, electrochemical, and theoretical methods. Additionally, the synthesized complexes have been evaluated for their antimicrobial activity, including antifungal and antibacterial properties, as well as for their industrial and environmental applications, specifically in dye degradation and photocatalysis.

Material and Methods

Reagents and instruments

2,5-dimethoxybenzaldehyde, M. W. (Molecular Weight) 166.17; 2-Amino-6-chloro-4-nitrophenol, M. W. 188.57 g/mol; $CoCl_2.6H_2O$ M. W. 237.93 g/mol; $NiCl_2.6H_2O$ M. W. 237.69 g/mol; $CuCl_2.2H_2O$ M. W. 170.48 g/mol; $ZnCl_2.2H_2O$ M. W. 172.38 g/mol of AR grade, ordered from Sigma. All chemicals are used without further purification. BRUKER Alpha-II FT-IR instrument the range between 400 cm^{-1} to 4000 cm^{-1} has been used for the measurement of FT-IR spectra. LABINDIA UV-3092 analytical UV–VIS Spectrophotometer have been used to detect absorption spectra in DMSO (5×10^{-4} M) at 25°C, range between 250 to 800 nm. JEOL Delta- 550 using TMS as internal reference have been used for NMR spectra (in DMSO-d6; 400 MHz Spectrometer). Digital conductivity meter of EI Delux model-601 used for the measurement of molar conductance in DMSO (1×10^{-4} M) at 25°C. Advances Brucker D-8 X-ray diffractometer has been utilized to obtain the Powder-XRD patterns with scanning range of 50–800,

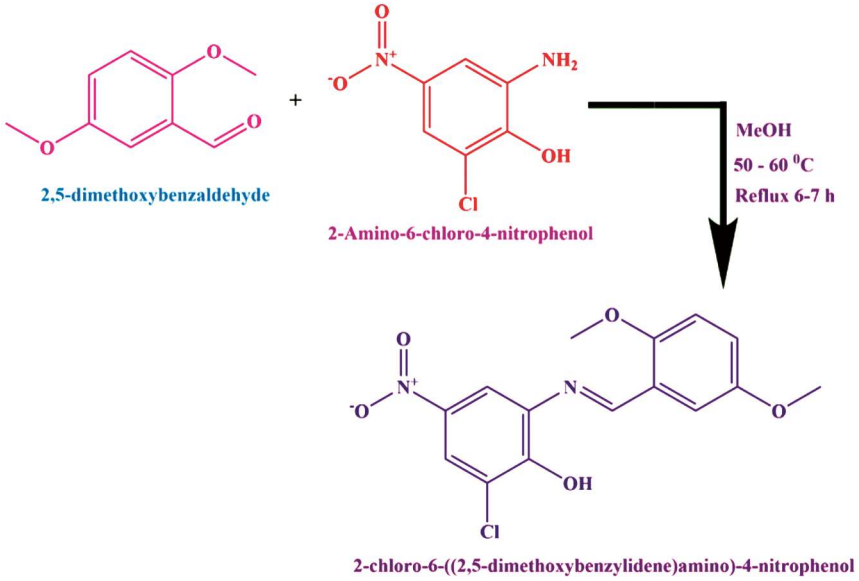

Fig. 1 — Synthesis of targeted bioactive ligand L

at 25°C. Thermo Scientific (FLASH 2000) CHN Elemental Analyzer has been used for elemental detection. Metrohm Autolab B.V. (PGSTAT128N) cyclic voltammeter at 25°C employed for cyclic Voltagrams. (Centre for Advanced Research (CAR)), Dr. H. S. Gour Vishwavidyalaya Sagar (M. P.), India. Model-Maldi-TOF Synapt XS HD Mass Spectrophotometer was used for mass spectra recorded on WATER'S Corporation, SAIF CSIR-Central Drug Research Institute Lucknow. EXSTAR, SII 6300 EXSTAR instrument in N_2 environment at 10 K min^{-1} heating rate up to 900 K at 25°C was used to record thermal data at Institute Instrumentation Centre IIT Roorkee, India.

Synthesis

Synthesis of bioactive ligand L; 2-chloro-6- ((2,5-dimethoxybenzylidene)amino)-4-nitrophenol

Methanolic solutions of 2,5-dimethoxy benzaldehyde (1.66 g, 10 mM) and 2-Amino-6-chloro-4-nitrophenol (1.88 g, 10 mM) were mixed in presence of an acid catalyst (Acetic acid) and refluxed at 50-60°C for 6-7 h. TLC was performed using toluene and ethanol to elucidate the proceedings of the reaction. Resulting substance was filtered out and washed with diethyl ether followed by methanol several times. The final product was dried and recrystallized by methanol. Preserved under vacuum environment over fused $CaCl_2$. (Fig. 1). Chem. For.: $C_{15}H_{13}ClN_2O_5$; M. W.: 336.73; Color: brick red; Yield: 75% (2.66g), m.p.: >330°C; stable; soluble in methanol, ethanol, $CHCl_3$ *etc.* strongly soluble in DMSO and DMF, insoluble in non-polar solvents. Molar conductance (DMSO) λm ($cm^2\Omega^{-1}mol^{-1}$): 17.3; UV–Vis (λ nm): 276, 403 nm; IR (KBr, cm^{-1}): 1689.02 ($\nu_{C=N}$ azomethine), 1156 (ν_{C-O}), 1153 (ν_{C-N}), 3400–3700 (ν_{O-H}), 3025-3200 (ν_{C-H} aromatic); ^{1}HNMR (400 MHz, DMSO-d_6) δ: 10.27 (s, –OH), 8.51 (s, –CH=N), 8.31-7.22 (m, aromatic protons), 3.4-3.8 (s, –OCH_3); Elemental Calcd. (%): C, 53.50; H, 3.89; Cl, 10.53; N, 8.32; O, 23.76; Found (%): C, 53.46; H, 3.91; Cl, 10.51; N, 8.34; O, 23.78; *m/z* (ESI-MS) Calcd. (amu): 336.70; Found (amu): 335.4.

Synthesis of the metal complexes [M $(L)_2$].2H_2O; (CoL, NiL, CuL) and ZnL)

1 mM methanolic solution of each divalent metal salt; Co (0.238 g), Ni (0.237 g), Cu (0.170 g), Zn (0.172 g) with 2mM methanolic solution of bioactive ligand L [(0.673 g)] in alkaline medium, continuously stirred and heated (50-60°C) for 4-5 h on magnetic hot plate stirrer. TLC eluted using toluene and ethanol. The colored constituted powder of each has been washed with methanol and diethyl ether several times. The final product has been dried and recrystallized by methanol. Preserved under vacuum environment over fused $CaCl_2$ (Fig. 2).

[Co $(L)_2$].2H_2O / CoL

Mol. For.: $C_{30}H_{28}Cl_2CoN_4O_{12}$; M. W.: 766.40; Color: Wine red; Yield: 74% (567.136 g); M.P.: >450°C; stable; soluble in DMSO and DMF; partially

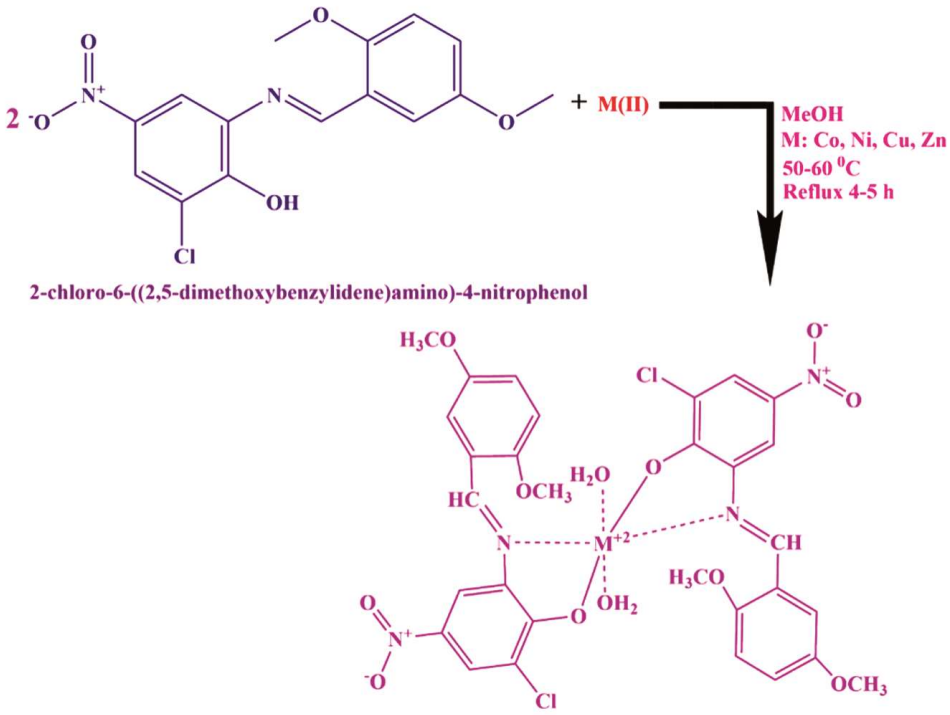

Fig. 2 — Synthesis of desired metal complexes (CoL, NiL, CuL, ZnL)

soluble in methanol, ethanol, $CHCl_3$ *etc.*, insoluble in non-polar solvents; Molar conductance (DMSO) λm ($Cm^2\Omega^{-1}mol^{-1}$): 25.4; UV–Vis (λ nm): 295, 381, 504; FT-IR (vib, cm^{-1}): 1676 ($\nu_{C=N}$ azomethine), 1253 (ν_{C-O}), 3250–3600 (ν_{O-H}), 490 (ν_{M-N}); Elemental Calcd. (%): C, 47.02; H, 3.68; Cl, 9.25; Co, 7.69; N, 7.31; O, 25.05; Found (%): C, 47.05; H, 3.66; Cl, 9.26; Co, 7.67; N, 7.33; O, 25.03; *m/z* (ESI-MS) Calcd. (amu): 766.40; Found (amu): 765.5.

[Ni $(L)_2$].2H_2O / NiL

Mol. For: $C_{30}H_{28}Cl_2NiN_4O_{12}$; M. W.: 766.16; Color: Pale yellow Yield: 71% (543.97 g); M.P.: >340°C; stable; soluble in DMSO and DMF; partially soluble in methanol, ethanol, $CHCl_3$ *etc.*, insoluble in non-polar solvents. Molar conductance (DMSO) λm ($Cm^2\Omega^{-1}mol^{-1}$): 26.4. UV–Vis (λ nm): 297, 375, 488; FT-IR (vib, cm^{-1}): 1666 ($\nu_{C=N}$ azomethine), 1142 (ν_{C-O}), 3250–3600 (ν_{O-H}), 485 (ν_{M-N}); Elemental Calcd. (%): C, 47.03; H, 3.68; Cl, 9.25; N, 7.31; Ni, 7.66; O, 25.06; Found (%): C, 47.01; H, 3.65; Cl, 9.24; N, 7.32; Ni, 7.69; O, 25.09; *m/z* (ESI-MS) Calcd. (amu): 766.16; Found (amu): 766.2.

[Cu $(L)_2$].2H_2O / CuL

Mol. For: $C_{30}H_{28}Cl_2CuN_4O_{12}$; M. W.: 771.01; Color: Reddish brown; Yield: 79% (609.09 g); M.P.: >440°C; stable; soluble in DMSO and DMF; partially soluble in methanol, ethanol, $CHCl_3$ *etc.*, insoluble in non-polar solvents; Molar conductance (DMSO) λm ($Cm^2\Omega^{-1}mol^{-1}$): 26.2. UV–Vis (λ nm): 299, 392, 515; FT-IR (vib, cm^{-1}): 1654 ($\nu_{C=N}$ azomethine), 1210 (ν_{C-O}), 3250–3600 (ν_{O-H}), 482 (ν_{M-N}); Elemental Calcd. (%): C, 46.73; H, 3.66; Cl, 9.20; Cu, 8.24; N, 7.27; O, 24.90; Found (%): C, 46.71; H, 3.63; Cl, 9.22; Cu, 8.22; N, 7.30; O, 24.92; *m/z* (ESI-MS) Calcd. (amu): 771.01; Found (amu): 772.1.

[Zn $(L)_2$].2H_2O / ZnL

Mol. For: $C_{30}H_{28}Cl_2ZnN_4O_{12}$; M. W.: 772.85; Color: Reddish brown; Yield: 76% (609.09 g); M.P.: >425°C; stable; soluble in DMSO and DMF; partially soluble in methanol, ethanol, $CHCl_3$ *etc.*, insoluble in non-polar solvents; Molar conductance (DMSO) λm ($Cm^2\Omega^{-1}mol^{-1}$): 27.4. UV–Vis (λ nm): 309, 402, 495; FT-IR (vib, cm^{-1}): 1570 ($\nu_{C=N}$ azomethine), 1154 (ν_{C-O}), 3250–3600 (ν_{O-H}), 487 (ν_{M-N}); Elemental Calcd. (%): C, 46.62; H, 3.65; Cl, 9.17; N, 7.25; O, 24.84; Zn, 8.46; Found (%): C, 46.59; H, 3.63; Cl, 9.19; N, 7.24; O, 24.86; Zn, 8.49; *m/z* (ESI-MS) Calcd. (amu): 772.85; Found (amu): 772.

Theoretical calculations

DFT is the most fundamental method to investigate the electronic structure of bioactive ligand L and its coordinated metal chelates (CoL, NiL, CuL, ZnL)[12].

Gaussian 16 has been employed for all the electronic calculations. Bioactive ligand L and its metal chelates were theoretically optimized by using DFT/B3LYP level 6–31G, and LANL2DZ basis set. The molecular structure of all the complexes have been optimized in gaseous phase applying the basic sets 6-31G and LANL2DZ. Bond lengths, angles between the bonds, HOMO & LUMO energy gap, Mulliken charges, MEP and global reactivity descriptors (*viz*: chemical potential, global softness, chemical hardness and electrophilicity index represented by μ, S, η and ω, respectively), were all defined molecular morphologies[13].

Biological applications

Antifungal assay

The antifungal activity of the bioactive ligand L and its divalent metal chelates was evaluated using the poisoned food technique against *F. oxysporum* and *A. niger*, with Bavistin as a standard fungicide[14]. Antifungal testing was conducted on 2% PDA media at various concentrations (100, 75, 50, and 25 mg/mL). The PDA media (Himedia) was prepared by dissolving 39 g in 1000 mL de-ionized water, boiling, and autoclaving for 20 min at 121°C. A stock solution (1000 mg/mL) was prepared in DMSO and diluted to the required concentrations, with DMSO (1 mL) as a negative control. The autoclaved solutions were added to conical flasks (media at 40°C), then poured into 9 cm petri dishes under aseptic conditions in a laminar flow hood with UV light for solidification. After solidification, 5 mm mycelial plugs from a two-week-old fungal colony were placed at the center of each treatment plate, which were incubated at 28°C until fungal growth in the control plates was nearly complete. Each treatment was conducted in triplicate[15]. The growth inhibition percentage (I) was calculated using Eq. (1).

$$\%\ \text{Growth inhibition (\% I)} = \frac{D_0 - D_t}{D_0} \times 100 \quad \ldots (1)$$

Where, Diameter of fungal colony was represented by D_t at various treatments and diameter of fungal colony with control represented by D_o.

Antibacterial assay

The antibacterial activity of the synthesized bioactive ligand L and its metal complexes was evaluated against *S. aureus* (ATCC6538) and *E. coli* (ATCC15224)[16] using the agar well-diffusion method. A bacterial suspension containing 106 CFU/mL of the test strain was spread evenly over the surface of nutrient agar plates. Wells (8 mm) were created using a sterile metallic borer, and 100 µL of test samples (1 mg/mL in DMSO) were added to the wells. DMSO was used as the negative control, and Streptomycin (1 mg/mL) served as the positive control. The plates were incubated at 37°C for 24 h. The antibacterial activity was determined by measuring the diameter of the zone of inhibition (mm)[17].

Antioxidant assay

2,2-diphenyl-1-picryhydrazyl (DPPH) scavenging effect 3.94 mg of 2,2-diphenyl-1-picryhydrazyl (DPPH) radical has been dissolved in 100 mL of methanol to prepare the solution. 0.2 mL of the bioactive ligand L and its coordinated metal (II) chelates solution with varying concentrations ranging from 250 to 2000 µg/mL have been added to 2.8 mL of the methanolic solutions of DPPH[18]. Utilizing the UV-Visible Spectrophotometer, the decrease in absorption of DPPH was observed at 517 nm after 45 min. The percentage inhibition was computed by comparing the actual absorption decrease to the control. As a reference, ascorbic acid is a renowned antioxidant. Every test and analysis was carried out twice, and the average of the results was obtained[19].

Dye degradation activities

The dye degradation measurements of L and its coordinated metal chelates have been examined by using methylene blue (MB) solution as organic pollutant at room temperature (298K). Samples of L and its metal chelates (50 mg/L) were poured to a solution of methylene blue (MB) in water (6 mg/L). Firstly the solution was stirred magnetically in the dark chamber for 30 min for ensure an adsorption/desorption equilibrium. These solutions have been kept under the UV light chamber with continuous stirring. At interval of 20 min, 3 mL of solution have been taken and analyzed by UV-Vis spectrophotometer. The adsorption of methylene blue decreases with the increasing of reaction time under UV light irradiation in the presence of catalyst[20]. Degradation of pure methylene blue also carried out under the same, for comparison. The % degradation of methylene blue was calculated by using Eq. (2).

$$\%\ Degradation = \frac{A_0 - A_t}{A_0}\ X\ 100 \quad \ldots (2)$$

Where A_0 and A_t are the absorbance of the solution at 0 and t min, respectively.

Table 1 — General information related to bioactive ligand L and its metal complexes.

Complexes molecular formula	Colour	Yield (%)	Molar Conductance ($\Omega^{-1}cm^2$ mol^{-1})	M.P. (°C)	Mol. Wt.	ESI-MS (Found)	Element Calcd. Found (Calculated) %					
							M	C	H	Cl	N	O
L	Dark red	79%	17.3	>330	336.73	335.4	_	53.46	3.91	10.51	8.34	23.78
CoL	Red brown	74%	25.4	>350	766.40	765.5	7.67	47.05	3.66	9.26	7.33	25.03
NiL	Brick brown	71%	26.4	>340	766.16	766.2	7.69	47.01	3.65	9.24	7.32	25.09
CuL	Red	79%	26.2	>340	771.01	772.1	8.22	46.71	3.63	9.22	7.30	24.92
ZnL	Pale yellow	76%	27.4	>325	772.85	772	8.49	46.59	3.63	9.19	7.24	24.86

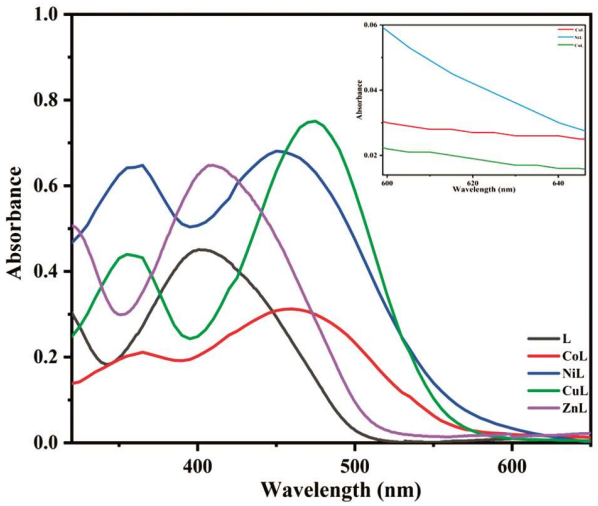

Fig. 3 — UV-Vis spectra of bioactive ligand L and its metal complexes

Results and Discussion

Molar conductivity

The molar conductance of synthesized bioactive ligand L and its coordinated metal chelates have been measured at 5 × 10^{-4} M concentration at room temperature in DMSO. The λ_m values were found in between 17.30 and 27.40 (cm^2 $\Omega^{-1}mol^{-1}$) confirm that the complexes were non-electrolytic in nature[21]. (Table 1).

Electronic absorption spectroscopy

The UV–Vis spectra of bioactive ligand L and its divalent metal complexes give an observable shifting of the electronic transition (Fig. 3). DMSO was used to analyze the electronic spectra. The bioactive ligand L absorbs at 276 nm, and 403 nm, which corresponds to π → π* and n → π* transition in aromatic ring and transition of non-bonding electrons of azomethine nitrogen (C=N) group respectively. It is observed for all the complexes, absorption bands shift to higher wavelength region viz. 295 nm,365 nm and 464 nm for CoL, 291 nm, 360 nm and 450 nm for NiL, 287 nm, 355 nm and 475 nm for CuL and 321 nm, and 411 nm for ZnL. The CoL and CuL metal complexes also represent low intensity band at 615 nm (16260 cm^{-1}) attributed to $T_1g \rightarrow T_1g$ (P); 625 nm (16000 cm^{-1}) assignable to $T_1g \rightarrow A_2g$ and 635 nm (15748 cm^{-1}) attributed to $Eg \rightarrow T_2g$ respectively, which are corresponding to d-d transition in metal complexes. The modification of π → π*, n → π* and d-d transition in metal complexes indicate the molecular environment transformation and chelation of bioactive ligand L with metal ions[22].

Infrared spectral studies of bioactive ligand L and its metal complexes

To determine the mode of chelation between the ligand L and metal ions, the infrared spectra of the free bioactive ligand L and metal complexes are compared. Table 2 represents the IR band allocations for bioactive ligand L and its metal chelates. Using the infrared spectra of the free bioactive ligand, band like ν (C=N) (azomethine) were used as a reference to identify the coordination sites that might be implicated in chelation. The bioactive azomethine linkage (-C=N) stretching vibration was identified as the source of the unique absorption band at 1689.02 cm^{-1} in the ligand's infrared spectra. The IR band caused by the azomethine group moves to the lower wave number 1654–1676 cm^{-1} upon complex formation, indicating that the azomethine nitrogen is involved in chelation with the metal ions. Broad bands were observed in the 3500–3700 cm^{-1} range by bioactive ligand L and its divalent metal complexes, which were linked to coordinated water molecules. Furthermore, a medium intensity band at 1142-1253 cm^{-1} corresponding to the methoxy's (C–O) stretching vibration was seen by the bioactive ligand L and its metal complexes. The discovery of

Table 2 — Important Infrared frequencies (cm^{-1}) of bioactive ligand L and its metal complexes.

Complexes	υOH	υ (C-H)	υ (C=N)	Phenolic υ (C-O)	υ (M-N)	υ (M-O)	υ (C-O) Methoxy
L	3400-3700	3025-3200	1689.02	1298.82	-	-	1156
CoL	3250-3600	2995-3190	1676	1263	490	565	1253
NiL	3250-3600	2990-3190	1666	1286	485	534	1142
CuL	3250-3600	2995-3195	1654	1290	482	577	1210
ZnL	3250-3600	2980-3200	1570	1271.4	487	579	1154

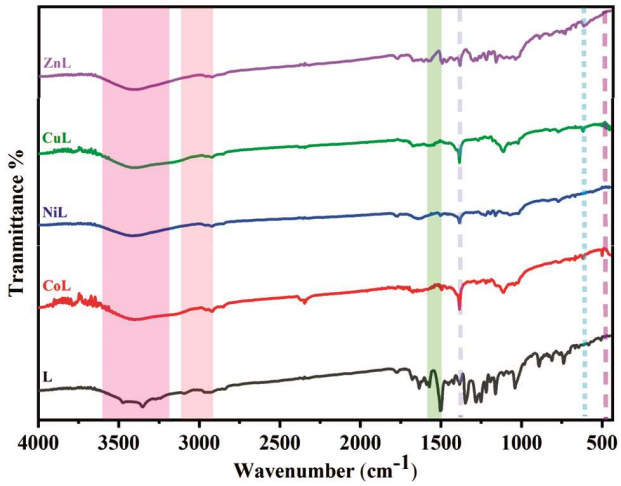

Fig. 4 — FT-IR (cm^{-1}) of bioactive ligand L and its metal complexes

additional bands in the spectra of the metal complexes at 534-579 cm^{-1} and 482-490 cm^{-1} attributable to ν (M-O) and ν (M-N), respectively, provided more proof of the coordination of the metal ion via the azomethine nitrogen atom and the hydroxyl oxygen atom. The metal ion is bound to two bidentate ligands, as the structure of the M^{2+} complex demonstrates, giving rise to distorted octahedral geometry. It is clear from the infrared spectra that the nitrogen and oxygen atoms of azomethine and hydroxyl group, respectively, serve as the pathways through which the metal ions chelate to the ligand (Fig. 4). To complete the geometry of the core metal ion, the coordinated water molecules satisfy the remaining coordination sites[23].

NMR studies of bioactive ligand L and ZnL

^{1}H NMR spectrum data is the evidence of the successful formation of the bioactive ligand L by the absence of signals characteristics of amino and aldehydic protons. Proton NMR spectrum of bioactive ligand L have been recorded in DMSO d6 with TMS as internal reference. In the ^{1}H spectrum of bioactive ligand L; phenolic -OH occur proton signal at 10.27 ppm (s, 1H) (Fig. 5). The most fundamental protonic signal at 8.51 ppm (s, 1H) is attributed to –CH=N. Other signals in the region 8.31-7.22 ppm (m, 5H) correspond to aromatic proton and methoxy group at 3.4- 3.8 ppm (s, 6H). The ^{13}C NMR spectrum of bioactive ligand L, display the signals in the region 112.6-139.2 ppm due to aromatic carbons. The peaks at 159.3 ppm appeared for azomethine carbon. The peak at 56.7-56.9 observed for methoxy carbon. All peaks were displayed in (Suppl. Fig. S1a)[24].

The ^{1}H NMR spectra of divalent metal complex ZnL gave additional information about complexation. In the ^{1}H NMR spectra of bioactive ligand, L showed a sharp peak, δ (-OH phenolic) at 10.27 ppm (s, 1H) which was absent in the spectra of the complexe ZnL indicating complex formation and deprotonation of ligand anion to metal ions. Suppl. Fig. S1b ZnL exhibited some similarities to the bioactive ligand, L with the most fundamental protonic signal at 8.51 ppm (s, 1H) is attributed to –CH=N. The signals for aromatic protons are in the region 8.31-7.22 ppm (m, 5H) and methoxy protons occur at 3.4-3.8 ppm (s, 6H).

In ^{13}C NMR, ZnL also displayed some similarities to the bioactive ligand, L. The region 112.6-139.2 ppm due to aromatic carbons, 159.3 ppm appeared for azomethine (–CH=N) carbon, and 56.7-56.9 ppm observed for methoxy carbon. (Suppl. Fig. S1c).

Mass spectral studies of bioactive ligand L and its metal complexes

The mass spectrum of bioactive ligand L represented a molecular ion peak at *m/z* 335.4 (calc. 336.7 amu). This equivalent to its mole. for. $C_{15}H_{13}ClN_2O_5$ as mentioned in (Table 1). It also displayed a pattern of peaks corresponding to several fragments and the most significant were at *m/z* 181.23 and 234.7 due to loss of $C_6H_2O_2NCl$ and C_7H_4N (calc. (intensity) 181.4 and 235.5), respectively. The ESI-MS results of $C_{30}H_{28}Cl_2CoN_4O_{12}$, $C_{30}H_{28}Cl_2N_4NiO_{12}$, $C_{30}H_{28}Cl_2CuN_4O_{12}$, $C_{30}H_{28}Cl_2ZnN_4O_{12}$ showed $[M-1]^+$ peak at *m/z* 765.5 (calc. 766.40 amu), 766.2 (calc. 766.16 amu), $[M+1]^+$ 772.1 (calc. 771.01 amu) and

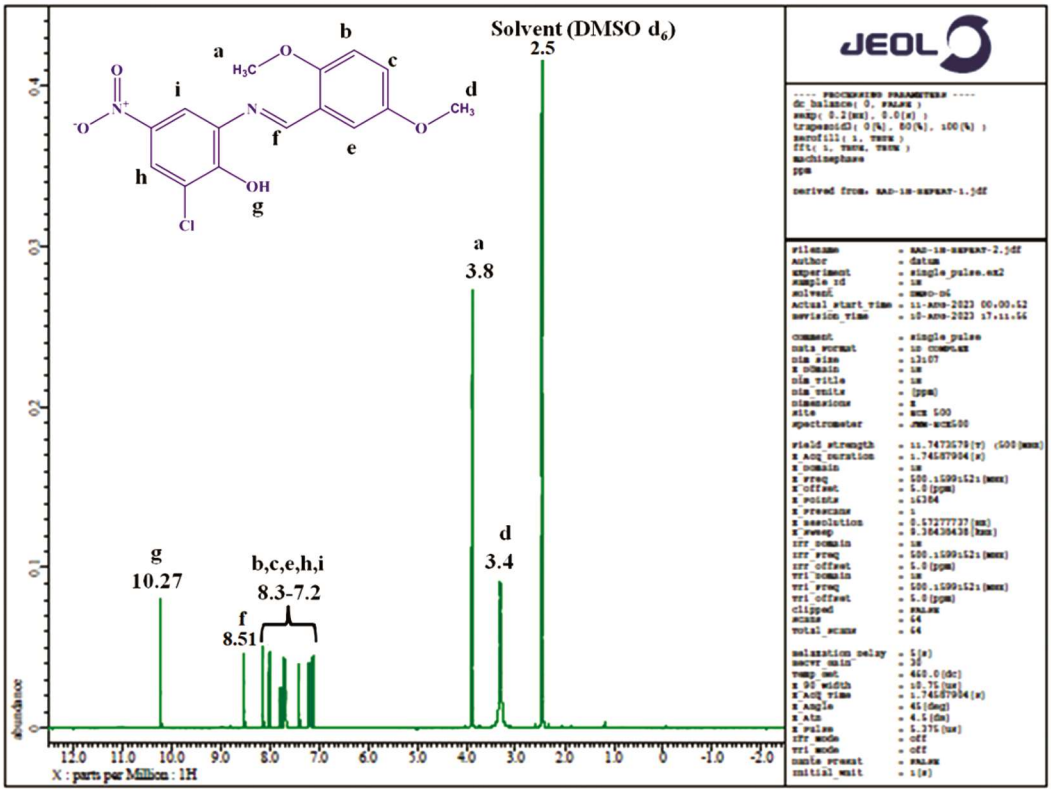

Fig. 5 — ^{1}H NMR of bioactive ligand L

772 (calc. 772.85 amu) equivalent to its mol. for. respectively. $C_{30}H_{28}Cl_2CuN_4O_{12}$ displayed a pattern of peaks; the most significant were at *m/z* 559.1, 610.8 and 685.8 due to loss of coordinated water molecules $C_{12}H_8O_2N_2$, $C_8H_9O_2$ and $C_{15}H_{13}NO_3Cl$, respectively. The ESI-MS spectra of metal chelates and bioactive ligand L shown in the (Suppl. Fig. S2a-e)[25].

Powder X-ray Diffraction analysis

There is no single crystal was observed for novel bioactive ligand L and its metal complexes. Hence, an X-ray powder diffraction pattern was obtained for bioactive ligand L and its metal complexes to detect the degree of crystalline nature. The working conditions of XRD can be listed as; scan step: 0.02°, scanning range: 5-80°, scanning mode: 2θ/θ. XRD diffraction patterns of bioactive ligand L and its metal complexes were given in (Fig. 6). Estimation of the grain sizes of the bioactive ligand L and its metal complexes with Scherrer's Eq. (3).

$$D = \frac{k\lambda}{\beta cos\theta} \quad \ldots (3)$$

λ represents X-ray wavelength, k = 0.94 represents spherical crystals, β represents full width of half maxima intensity, θ represents Bragg's diffraction angle. The average grain sizes (D) of the bioactive ligand L and its metal complexes have been calculated from the highest peak intensity.

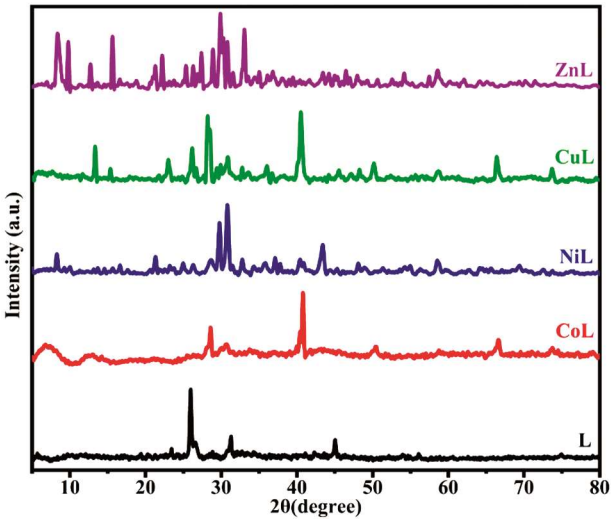

Fig. 6 — Powder X-ray Diffraction analysis of bioactive ligand L and its metal complexes

X-ray Diffraction analysis of bioactive ligand L

The X-ray diffraction behavior of the bioactive ligand L and its metal complexes shows several peaks having high intensities. These peaks can be listed in

Table 3 — Crystal parameters of bioactive ligand L and its metal complexes.

Samples	2θ	β	d-spacing	Crystalline size	Avg crystalline size
L	25.96	0.30	3.42	26.43	30.20
CoL	40.77	0.32	2.21	26.36	14.65
NiL	30.81	0.41	2.89	19.90	23.04
CuL	40.52	0.46	2.22	18.06	20.60
ZnL	29.99	0.58	2.97	14.10	24.25

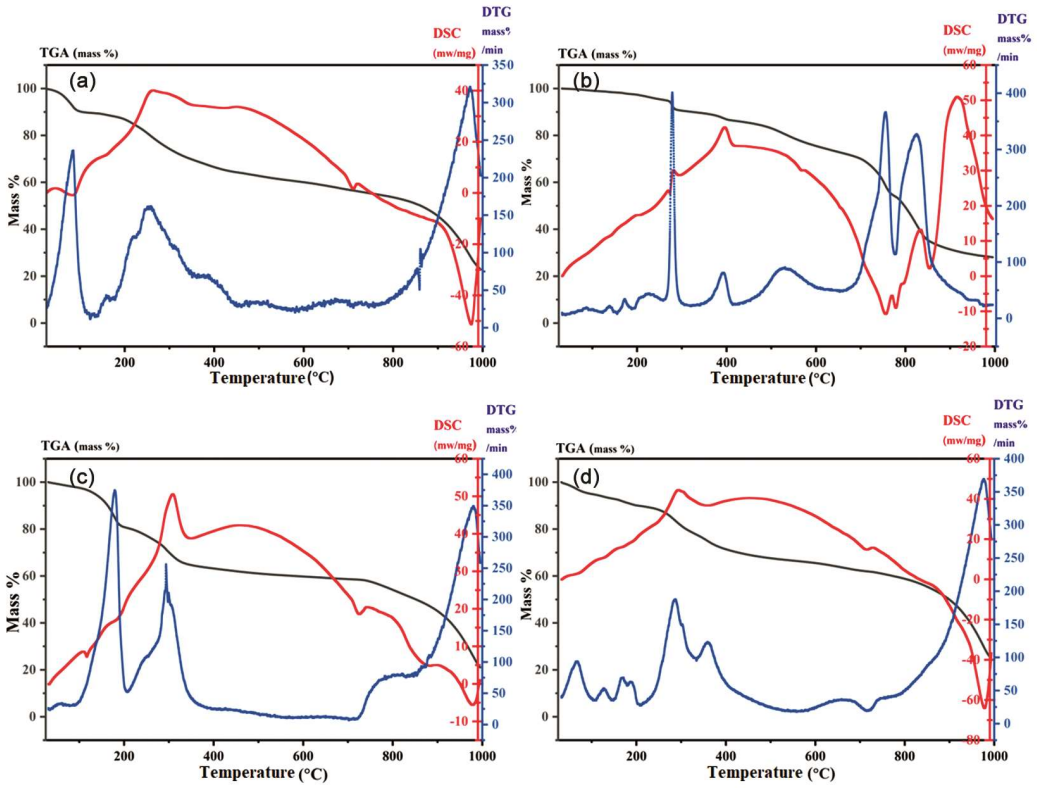

Fig. 7 — Thermograms of metal complexes (a) CoL, (b) NiL, (c) CuL, (d) ZnL

supplementary data. The highest and lowest intensities were found at the peak of 25.96° and 28.85° respectively. The average crystalline size of bioactive ligand L and its metal complexes have been obtained at 30.20 nm, 14.65 nm, 23.04 nm, 20.60 nm, and 24.25 nm respectively. Collected data represents 2θ, full width half maxima (β), d-spacing and crystalline size (D) are mentioned in (Table 3)[26]. The brief discussion provided in supplementary data (Suppl. Table S1a-e).

Thermolgravimetric analysis

Thermal stability of the metal complexes (CoL, NiL, CuL, ZnL) is governed by a crucial technique, temperature range from room temperature to 1000°C, the heating rate in most of the cases being 10°/min. The analysis was performed in N_2 environment. Thermogravimetric analysis (TGA) was analyzed to get an idea about the water and chelating parts are lattice/outside the coordination sphere or inside the coordination sphere. This is also useful for identification of molecular structure and the different types of solvent of crystallization. Thermogravimetric (TG) and differential thermogravimetric (DTG) analyses were performed metal complexes. The thermograms of the synthesized metal complexes (CoL, NiL, CuL, ZnL) can be subdivided into three main decomposition stages as shown in (Fig. 7) and observed outcomes were concluded in (Table 4). In first degradation stage of metal complexes temperature range up to 200°C, elimination of lattice water as well as coordinated water molecules. In second degradation stages of metal complexes temperature range up to 500°C, elimination of non-

Table 4 — Steps of thermal decomposition of metal complexes (CoL, NiL, CuL, ZnL).

Samples	Temp. range (°C)	DTG peak (°C)	Wt. loss (%) Found	Wt. loss (%) Cal.	Lost fragments (no. of molecules)	Residues (%) MO	Residues (%) By products Found	Residues (%) By products Cal.
CoL	23-193	78.01	12.7	12.9	Two molecules of lattice water Two molecules of coordinated water	CoO	12.42	12.43
	193-500	261.79	24.6	27.7	Non-chelating part of ligand			
	500-995	970.49	40.5	37.2	Chelating part of ligand			
NiL	32.3-289	162.2	9.1	9.4	Two molecules of lattice water Two molecules of coordinated water	NiO	18.25	18.23
	289-799	395.08	20.9	19.9	Non-chelating part of ligand			
	799-995	914.56	42.0	44.82	Chelating part of ligand			
CuL	31.2-186	115.58	17.4	17.7	Two molecules of lattice water Some other chelating part of ligand	CuO	10.98	10.95
	186-600	308.98	22.8	22.3	Non-Chelating part of ligand			
	600-994	974.56	44.5	44.7	Chelating part of ligand			
ZnL	32-200	169.83	9.9	9.3	Two molecules of lattice water Two molecules of coordinated water	ZnO	14.37	14.35
	200-600	291.74	24.6	24.7	Non-chelating part of ligand			
	600-993	976.29	40.6	40.4	Chelating part of ligand			

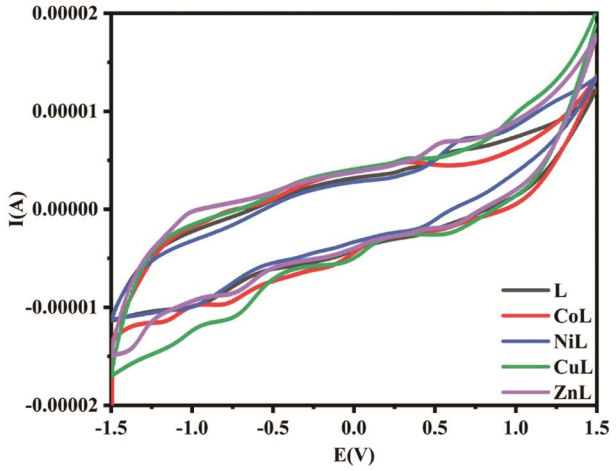

Fig. 8 — Cyclic Voltammogram of synthesized bioactive ligand L and its metal chelates

chelating part of the ligand. In third degradation stages of metal complexes temperature range up to 995°C, elimination of chelating part of the ligand. The final stages conclude the formation of corresponding metal oxides and pyrolyzed residual by-products. The interpretation of melting points using DSC curve have been found the temperature range 300-400°C for all the synthesized metal complexes, which were concluded by endothermic packs[27].

Cyclic voltammetry (redox properties)

The electrochemical investigations were performed by using cyclic voltammetry (CV) technique. The current or voltage is monitored by sweeping the potential back and forth (from positive to negative and vice-versa) between the selected limits. Migration of ions in the solution maintains electron neutrality while performing the CV, electrons move from the electrode to analyte to compensate the charge and close the electric circuit. A conventional three electrode system; working electrode, reference electrode, and counter electrode were commonly used in CV. Electrochemical properties of newly synthesized compounds have been studied containing a 0.005M solution of bioactive ligand, L and corresponding metal coordinated complexes, (CoL, NiL, CuL, ZnL), in DMSO solution concentration with 0.05M of Tetra Butyl Ammonium Perchlorate (TBAP) used as a supporting electrolyte. The scanning potential ranged between -1.5 to +1.5 V with scanned rate 100 mVs^{-1}. All experiments have been performed at room temperature under N_2 atmosphere. The CV of bioactive ligand L (Epa = 0.499 V, Epc = -0.752 V; $\triangle E$ = Epa-Epc = 0.253 V) shows a quasi-reversible peak for the couple of azomethine (C=N) bond and functional groups associated with bioactive ligand L. The CV graph of all the compounds have been shown in (Fig. 8). The divalent metal complexes CoL. NiL, CuL, ZnL also performs comparable behavior in CV graph, which offers a redox couple. The scanning potential ranged between -1.5 to +1.5 V with scanned rate 100 mVs^{-1}. The observed CV data have been discussed in (Table 5). The degree of reversibility of a reaction can be

Table 5 — CV evaluation of synthesized bioactive ligand L and its metal complexes.

Sample	Epa (V)	Epc (V)	ΔE (V)	Ia	Ic	Ia/Ic	$\Delta E_{1/2}$ (V)
L	0.499	-0.752	-0.253	5.943	-7.691	0.772	0.625
CoL	0.447	-0.781	-0.334	4.986	-6.507	0.766	0.614
NiL	0.521	-0.777	-0.255	5.994	-8.019	0.747	0.649
CuL	0.452	-0.783	-0.331	5.565	-7.512	0.740	0.618
ZnL	0.495	-0.796	-0.300	6.697	-8.845	0.7571	0.646

Table 6 — Growth inhibition % of synthesized bioactive ligand L along with metal chelates.

Compounds	Growth Inhibition %	
	Fusarium oxysporum	*Aspergillus niger*
Control	0	0
Bavistin	98.5	97.68
DMSO	42.64	41
L	70.07	78.41
CoL	71.32	77.21
NiL	61.34	76.85
CuL	76.3	80.81
ZnL	73.81	74.82

ascertained by comparing the back and forth peak potentials. The ratio between the scan rate ($I_{pc}/v^{1/2}$) and the cathodic peak current is nearly constant, which reveals, the process controlled by diffusion. There is a small correlation between the scan rate and peak potential. The ratio of Ia/Ic was less than one or near to unity clarifies this redox couple is a one electron transfer reaction. From these results it can be concluded that metal complexes CoL. NiL, CuL, ZnL gave quasi-reversible one-electron transfer process controlled by diffusion[28].

[a] ΔE (V) = Epa-Epc, [b]$E_{1/2}$ (V) = Epa+Epc

Bio-assay investigations

In vitro antifungal activity

All the synthesized complexes tested against two fungal strains; *F. oxysporum* and *A. niger* by applying poisoned food technique. Bavistin have been used as reference drug in this assay. Activity parameters are determined by % growth inhibition; the significant activity observed above 70% growth inhibition, good activity observed between 60-70% growth inhibitions, moderate activity observed between 50-60% growth inhibition and non-significant activity observed less than 50% growth inhibition. The final investigation shows that copper complex (CuL) have significant activities against both the fungus. The results are shown in (Table 6). In general, the metal complexes perform the better activity than ligand L due to their lipophilic nature. Such increased in reactivity of metal complexes can be explained by Tweedy's chelation theory. The polarity of metal ion reduces due to overlapping with ligand's orbital, which results the metal complexes penetrate easily into the lipid membranes and the enzymatic cites of microorganism[29]. All compounds have been tested at different concentrations. The significant results show at concentration 75% where the minimum growth of fungus has been observed (Fig. 9).

Sheena Mohan *et al*. reported the synthesis, crystal structure, spectral characterization, and antimicrobial studies of the compound. The antifungal activity of DMBDPP (Ligand) was assessed against two fungal cultures *A. niger and Candida albicans* by Potato Dextrose agar plates using agar well diffusion method for three concentrations (25, 50, 100 µg/mL) using a standard Clotrimazole. Against both *A. niger* and *C. albicans*, DMBDPP shows no activity at lower concentration of 25 µg/mL. But at higher concentration (of 100 µg/mL, 10 and 13 mm zone of inhibition respectively) DMBDPP shows comparable activity against both the organisms.

Antibacterial activity

In vitro antibacterial activity has been tested against two bacterial strains: Gram-positive and Gram-negative *S. aureus* and *E. coli*, respectively using Streptomycin as standard drug. The agar well-diffusion method have been used, each experiment was carried out in triplicate. First antibacterial susceptibility assay was performed then antimicrobial sensitivity assay (MIC) was carried out. All the compounds show the susceptibility (at 100% concentration), where as the value of minimum inhibition concentration (MIC) found at 50% concentration (Fig. 10). The copper complex performed better antibacterial activity against both the bacterial strains. The least activity performed by ligand against both the bacterial strains. In general metal complexes perform better biological activity than parental ligands (Table 7). This increasing in reactivity of metal complexes can be explained by

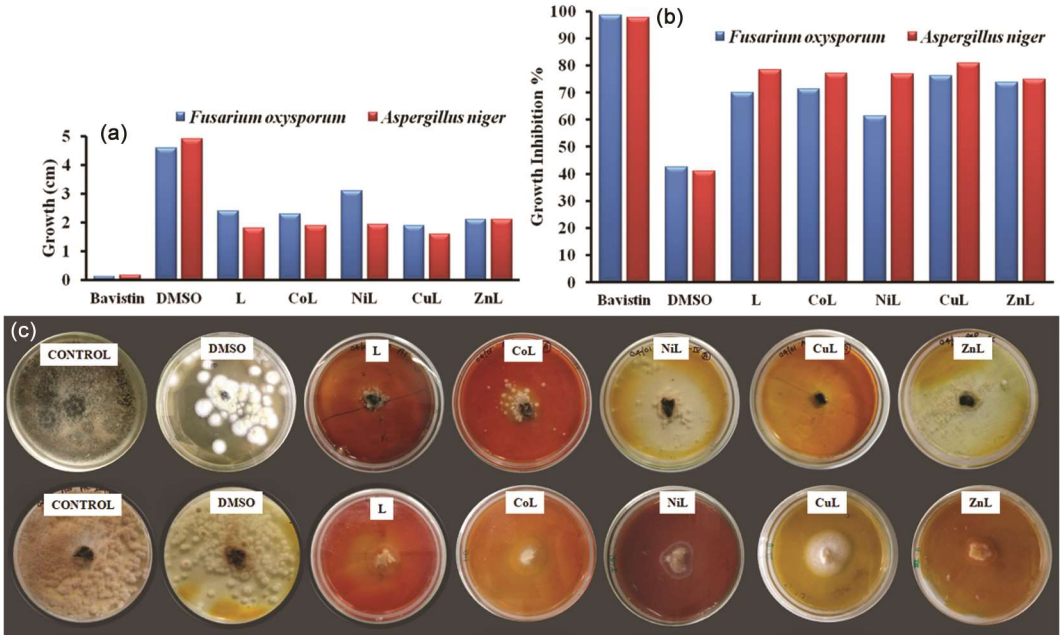

Fig. 9 — (a) Graphical representation; and (b) Growth inhibition % and (c) Pictorial representation of synthesized bioactive ligand L and its metal chelates against two fungal strains; *F. oxysporum* and *A. niger*

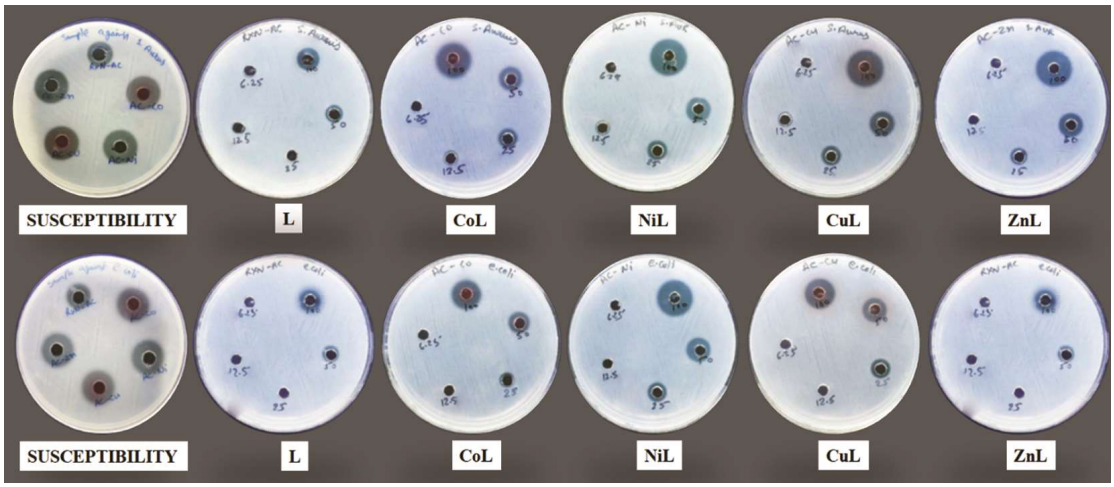

Fig. 10 — Graphical representation of inhibition zones of synthesized bioactive ligand L and its metal complexes against two bacterial strains: *S. aureus* and *E. coli*

Table 7 — Zone of inhibition of synthesized bioactive ligand L and its metal chelates.

Compounds	Zone of inhibition (mm)			
	Staphylococcus aureus		*Escherichia coli*	
	Susceptibility (100% conc)	MIC (50%)	Susceptibility (100% conc)	MIC (50%)
L	15	8	14	9
CoL	18	12	16	11
NiL	17	11	13	13
CuL	19	13	17	14
ZnL	18	12	17	10
Streptomycin	26	20	28	19

Tweedy's chelation theory which is based on polarity. Results the metal complexes penetrate easily into the lipid membranes or the enzymatic cites of microorganism[30].

Sheena Mohan *et al*. reported the synthesis, crystal structure, spectral characterization, and antimicrobial studies of the compound. In comparison to 10 µg of Streptomycin, the ligand DMBDPP showed no activity at the lower concentration of 25 µg/mL against Gram-negative bacteria. But at higher concentration of 100 µg/mL, DMBDPP shows good activity against *E. coli (*13 mm*), P. aeroginosa* and *K. pneumonia*. DMBDPP shows moderate activity against Gram-positive bacteria at medium and higher concentration. *S. aureus (*16 mm).

Antioxidant activity

The reducing nature of the synthesized compounds have been examined by their interaction with the free stable radical 1,1-diphenyl-2-picryl-hydrazyl (DPPH) at four different concentrations (250-2000 µg/mL) at 30 min. 1,1-diphenyl-2-picryl-hydrazine can be produced by antioxidants reacting with DPPH. DPPH exhibits a prominent absorption band at 517 nm with appearance a deep violet color because of its odd electron. In the presence of a free radical scavenger this odd electron becomes paired. Results the absorption decreased and the decolorization of the compounds. Change of absorbance is assessed to evaluate the antioxidant potential of complexes. This assay functions well as a primary screening system. All the compounds compared with ascorbic acid, used as standard antioxidant. It is found that the CuL and ZnL have been found highest and lowest interaction with DPPH at all the concentrations. The interaction is directly proportional to concentration and time of the tested compounds. Figure 11 represented the order of scavenging abilities as follows: Ascorbic acid > CuL > L > NiL > CoL > ZnL[31].

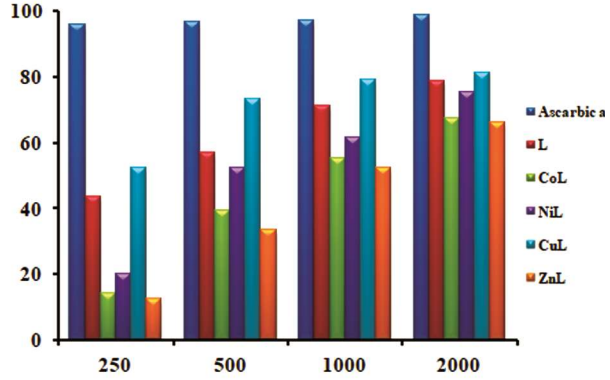

Fig. 11 — DPPH scavenging ability of bioactive ligand L and its metal complexes

Geometry optimization

In the field of computational chemistry there are so many processes for energy minimization and finding the arrangement of atom in space where the net inter-atomic force on each atom is almost zero. One of the quantum mechanical (QM) methods, density functional theory (DFT) is used to calculate the geometry of atoms and molecules. DFT calculations at the B3LYP/6-31G level and LANL2DZ basic sets have been carried out for all the compounds. DFT explore the electronic structure of L and its metal complexes (CoL, NiL, CuL, ZnL) including level of atoms, symbols, bond lengths, bond angles and dihedral angles. The most significant data are mentioned below (Table 8a-e)[32].

The optimized results confirmed that the binding of metal ions with N (azomethine) and O (phinolic) of parent compound or bioactive ligand L. The elongation or compression of bond lengths, formation of new bonds as well as formation of new bond angles in case of metal coordinated complexes have been mentioned in (Table 8a-e). Metal coordination also affects the bond angles represented in (Fig. 12).

Mulliken Charges

Mulliken charges give the information about the mulliken populations, which provides estimating partial atomic charges. The computational method is based on the linear combination of atomic orbitals molecular orbital method. Mulliken charges depicts the electron density which leads the polarization and finally the dipole moment of the molecules. There are two sites are available in bioactive ligand L for the coordination with metal ion. Atomic level N11 (azomethine) and O9 (phinolic) show the value of mulliken charges -0.115 and -0.488 respectively. The negative values of electrostatic potential confined the presence of active sites. Electrostatic potential discussed below[33].

Molecular electrostatic potential (MEP)

MEP is the interaction energy between the charge distribution and a unit positive charge of a molecule. MEP recognized the sites for nucleophilic and electrophilic reactions as well as weak van der waals force of attraction. These sites are suitable for bioactivities. Electron density on molecular surface is different to each other. The Π electron density easily distinguishes through the MEP diagram (Fig. 13). The

Table 8 — (a) Important bond lengths of bioactive ligand L

L			
Level of atoms	Bond lengths (Å)	Level of atoms	Bond angles (°)
N (11)C (12)	1.28	C (3)N (11)C (12)	128.23
C (3)N (11)	1.39	N (11)C (12)C (14)	123.50
C (12)C (14)	1.45	C (12)C (14)C (15)	166.39
C (17)O (24)	1.39	C (3)C (4)O (9)	117.84
C (4)O (9)	1.35		
C (5)Cl (33)	1.80		
C (1)N (34)	1.45		

Table 8 — (b) Important bond lengths of CoL

CoL			
Level of atoms	Bond lengths (Å)	Level of atoms	Bond angles (°)
N (9)C (10)	1.31	N (9)Co (26)O (29)	91.65
C (3)N (9)	1.43	O (29)Co (26)O (27)	83.89
C (10)C (12)	1.47	O (27)Co (26)N (28)	84.62
C (14)O (68)	1.39	N (28)Co (26)O (31)	91.59
C (2)O (21)	1.31	O (31)Co (26)O (21)	91.58
C (1)Cl (22)	1.81	O (21)Co (26)N (9)	86.58
C (5)N (23)	1.450	O (29)Co (26)O (31)	174.86
N (28)C (43)	1.30		
N (28)C (35)	1.43		
C (43)C (44)	1.47		
C (45)O (58)	1.39		
N (9)Co (26)	1.98		
O (21)Co (26)	1.92		
Co (26)O (29)	2.27		
Co (26)O (31)	2.25		
Co (26)N (28)	1.97		
Co (26)O (27)	1.92		

Table 8 — (c) Important bond lengths of NiL

NiL			
Level of atoms	Bond lengths (Å)	Level of atoms	Bond angles (°)
N (9)C (10)	1.312	N (9)Ni (26)O (29)	64.87
C (3)N (9)	1.436	O (29)Ni (26)O (27)	79.26
C (10)C (12)	1.470	O (27) Ni (26)N (28)	85.59
C (14)O (68)	1.394	N (28) Ni (26)O (31)	67.35

(*Contd.*)

Table 8 — (c) Important bond lengths of NiL (*Contd.*)

NiL			
C (2)O (21)	1.342	O (31) Ni (26)O (21)	79.35
C (1)Cl (22)	1.808	O (21) Ni (26)N (9)	86.19
C (5)N (23)	1.461	O (29) Ni (26)O (31)	178.36
N (28)C (43)	1.309		
N (28)C (35)	1.435		
C (43)C (44)	1.473		
C (45)O (58)	1.397		
N (9)Ni (26)	1.928		
O (21)Ni (26)	1.862		
Ni (26)O (29)	2.278		
Ni (26)O (31)	2.260		
Ni (26)N (28)	1.930		
Ni (26)O (27)	1.879		

Table 8 — (d) Important bond lengths of CuL

CuL			
Level of atoms	Bond lengths (Å)	Level of atoms	Bond angles (°)
N (9)C (10)	1.316	N (9)Cu (26)O (29)	53.67
C (3)N (9)	1.427	O (29)Cu (26)O (27)	64.34
C (10)C (12)	1.465	O (27)Cu (26)N (28)	79.98
C (14)O (68)	1.389	N (28)Cu (26)O (31)	83.10
C (2)O (21)	1.484	O (31)Cu (26)O (21)	72.53
C (1)Cl (22)	1.811	O (21)Cu (26)N (9)	69.59
C (5)N (23)	1.454	O (29)Cu (26)O (31)	169.75
N (28)C (43)	1.309		
N (28)C (35)	1.521		
C (43)C (44)	1.473		
C (45)O (58)	1.391		
N (9)Cu (26)	1.852		
O (21)Cu (26)	1.900		
Cu (26)O (29)	2.269		
Cu (26)O (31)	2.270		
Cu (26)N (28)	1.970		
Cu (26)O (27)	1.898		

(*Contd.*)

Table 8 — (e) Important bond lengths of ZnL

ZnL			
Level of atoms	Bond lengths (Å)	Level of atoms	Bond angles (°)
N (9)C (10)	1.314	N (9)Zn (26) O (29)	94.11
C (3)N (9)	1.421	O (29) Zn (26)O (27)	76.34
C (10)C (12)	1.472	O (27) Zn (26)N (28)	84.53
C (14)O (68)	1.392	N (28) Zn (26)O (31)	86.54
C (2)O (21)	1.310	O (31) Zn (26)O (21)	97.40
C (1)Cl (22)	1.812	O (21) Zn (26)N (9)	88.62
C (5)N (23)	1.449	O (29) Zn (26)O (31)	171.86
N (28)C (43)	1.309		
N (28)C (35)	1.427		
C (43)C (44)	1.471		
C (45)O (58)	1.394		
N (9)Zn (26)	1.860		
O (21) Zn (26)	2.010		
Zn (26)O (29)	2.192		
Zn (26)O (31)	2.172		
Zn (26)N (28)	1.967		
Zn (26)O (27)	2.054		

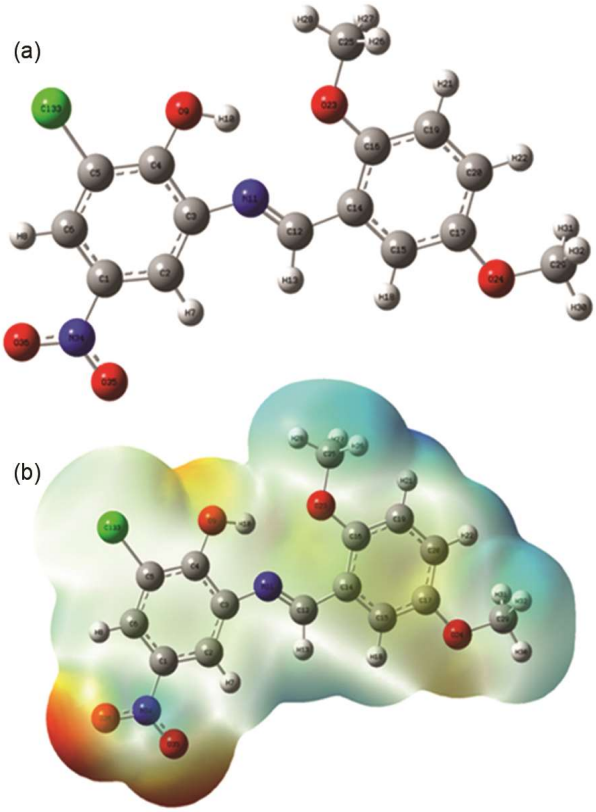

Fig. 13 — (a) Optimized geometry of bioactive ligand L; and (b) Diagrammatic representation of molecular electrostatic potential (MEP)

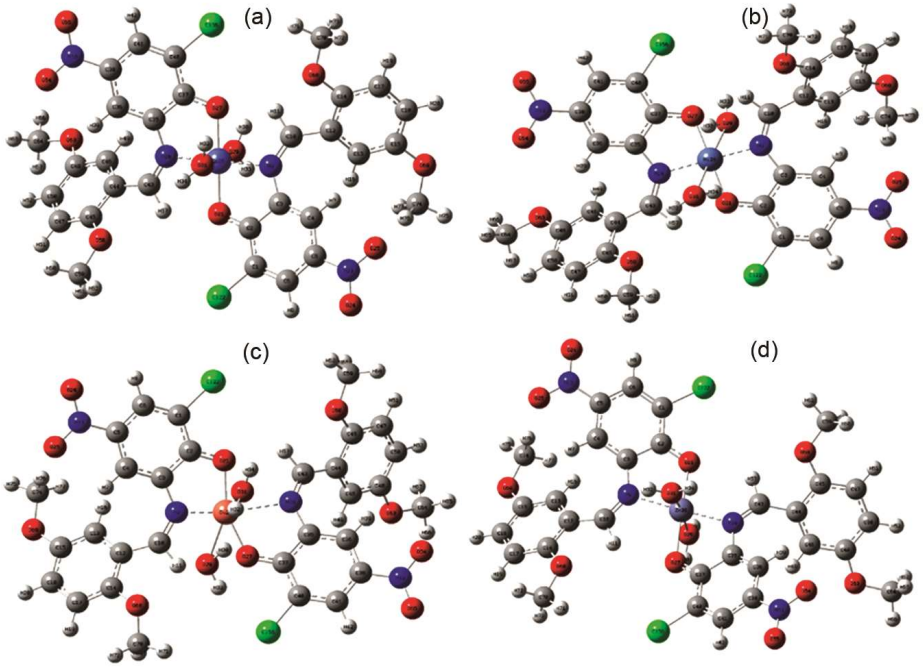

Fig. 12 — Optimized geometries of metal complexes (a) CoL; (b) NiL; and (c) CuL, (d) ZnL

electrostatic potential surface also observed by different colors as follows; red < orange < yellow < green < blue. Moving red to blue increases the electrostatic potential (decrease the electron density). In bioactive ligand L there are two donor atoms N11 (azomethine) and O9 (phenolic) show reddish-yellow color which denote electron density both the donor atoms as well as negative potential region[34].

HOMO-LUMO Analysis (FMO)

Frontier molecular orbital (FMO) describe the occupation of electron in HOMO and LUMO. The highest energy, occupied molecular orbital easily donate the electron act as nucleophile and the lowest energy, unoccupied molecular orbital easily accepts the electron act as electrophile. The energy difference (ΔE) between HOMO and LUMO calculated as ($\Delta E=E_{HOMO}-E_{LUMO}$). Smaller the HOMO-LUMO gap higher the reactivity, higher the thermodynamic stability as well as better biological activity[35]. ΔE shown in (Fig. 14).

Global Chemical reactivity descriptors

DFT based global chemical reactivity descriptors like electrophilicity index (ω), chemical hardness (η), chemical potential (μ) and global softness (s) have been calculated from HOMO-LUMO energies using koopman's theorem. These descriptors are used to understand the relationship between stability, structure, biological activities and chemical reactivity of synthesized compounds. Lower the softness value, lower the polarization and lower the biological activity and global chemical reactivity shown in (Table 9).

Dye degradation measurements

The absorbance of methylene blue gradually decreases with the increasing of reaction time under the UV light in the presence of catalysts L and its coordinated metal chelates CoL, NiL, CuL, ZnL). The measured percentage of degradation of methylene blue has been shown in (Fig. 15). Above observations depicts that, the degradation performance of the complexes is different and the CuL is the better one. The least degradation activity shows by bioactive ligand L. The degradation of organic pollutants has been carried out in the same manner. The degradation rate of methylene blue observed within 120 min under UV lamp irradiation. The explanation of L and its coordinated metal chelates (CoL. NiL, CuL, ZnL) are described under subpoints[36].

UV-DRS measurements

UV-DRS (Diffuse Reflectance Spectroscopy) serve as an effective method for analyzing the electronic characteristics of methylene blue dye, especially when assessing the impact of solid catalysts on its

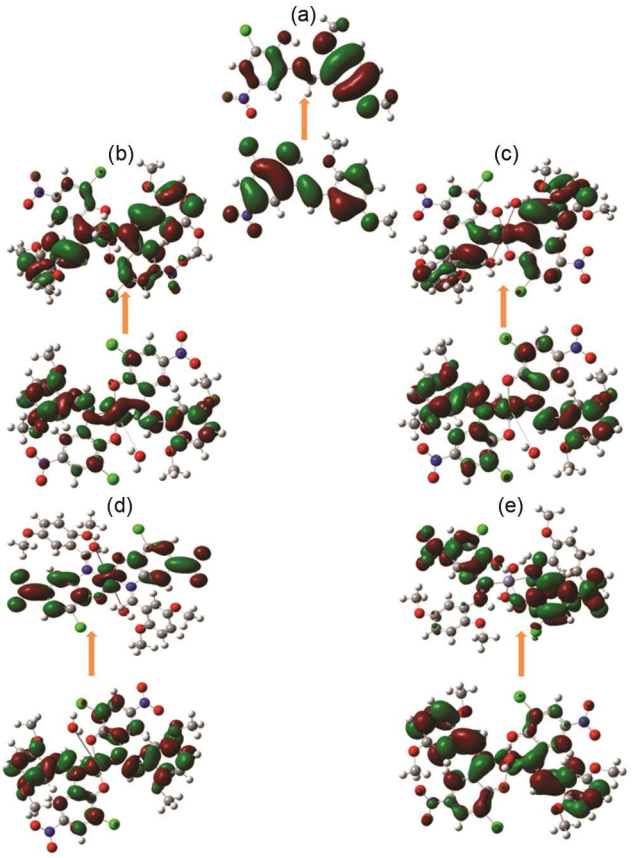

Fig. 14 — HOMO-LUMO orbitals of (a) Bioactive ligand L; (b) CoL; (c) NiL; (d) CuL; and (e) ZnL

Table 9 — Tabular representation of HOMO-LUMO energy gap (ΔE), global reactivity descriptors and dipole moment

Compounds	($\Delta E=E_{HOMO}-E_{LUMO}$) (ev)	μ (ev)	η (ev)	s (ev)	ω (ev)	Dipole moment (Debye)
L	3.1938	4.784	1.597	0.313	7.166	8.774
CoL	2.946	4.297	1.473	0.339	6.267	4.236
NiL	2.949	4.658	1.474	0.339	7.359	4.360
CuL	2.692	4.692	1.346	0.371	8.025	4.356
ZnL	3.126	4.362	1.584	0.316	6.006	4.358

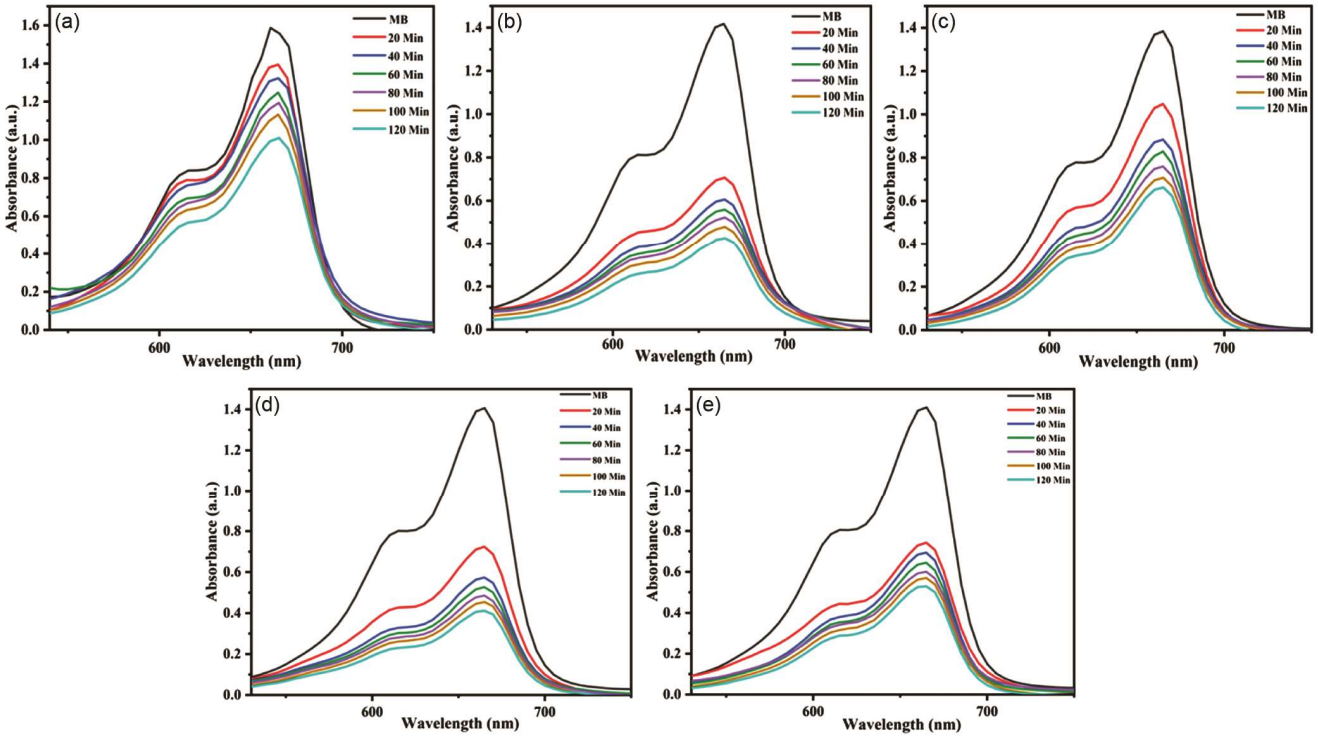

Fig. 15 — Absoption spectra of MB in presence of (a) Bioactive ligand L; (b) CoL; (c) NiL; (d) CuL; and (e) ZnL

degradation. The dye exhibits clear absorption band, mainly around 665 nm, due to its π-π* transitions. The introduction of bioactive ligand L and its metal complexes can lead to noticeable changes in these absorption bands and their intensities, indicating a modification in the dye's electronic environment (Suppl. Fig. S3). Furthermore, the reflectance data can be interpreted to calculate the direct band gap of methylene blue, measured for bioactive ligand L and its metal complexes (CoL, NiL, CuL, ZnL) at 4.97 eV, 4.24 eV, 4.55 eV, 4.02 eV and 4.30 eV respectively. The reduction in the band gaps (L > NiL > ZnL > CoL > CuL), as determined from the DRS results, suggests improved electron mobility and reactivity (L < NiL < ZnL < CoL < CuL), thereby enhancing the degradation process of the dye[37].

Effect of pH

Figure 16 shows the effect of pH on dye degradation of MB using bioactive ligand L and its metal complexes (CoL, NiL, CuL, ZnL) as a degradant. The pH of the MB solution decreased under UV light irradiation. Degradation of the tested solutions of MB have been studied in the pH range 4-11 followed by UV irradiation for interval 20 min with 50 mg/L bioactive ligand L and its metal complexes. The pH of reaction mixture has been

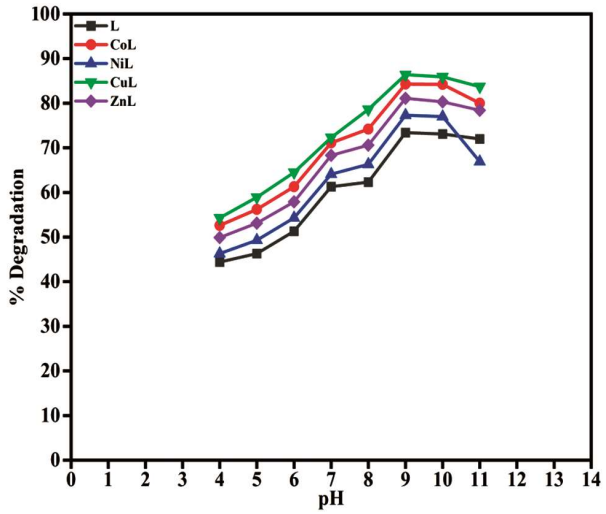

Fig. 16 — Degradation of MB at different pH at room temperature

adjusted by 1 M HNO_3 or 1 M NaOH. It is observed that the acidic pH was inhibited the dye degradation while the basic pH favored. The highest degradation was obtained at pH 9. The low activity obtained at acidic condition can be due to strong interaction of the dye molecules on the active site[38].

Effect of initial concentration of dye

The impact of MB dye concentration on its degradation has been investigated. Table 10 and

Table 10 — Statistical representation of initial concentration of dye

Dye concentration (PPM)	% Degradation				
	L	CoL	NiL	CuL	ZnL
10	56.11 ± 0.67	90.92 ± 0.66	73.04 ± 0.63	91.41 ± 0.57	82.97 ± 0.74
20	48.34 ± 0.73	86.6 ± 0.69	68.62 ± 0.73	87.94 ± 0.63	79.87 ± 0.52
30	45.22 ± 0.63	83.12 ± 0.71	65.65 ± 0.65	85.53 ± 0.62	77.75 ± 0.63
40	41.21 ± 0.71	80.28 ± 0.75	59.85 ± 0.53	82.76 ± 0.51	74.75 ± 0.66
50	38.91 ± 0.77	77.44 ± 0.67	56.04 ± 0.51	79.71 ± 0.64	70.85 ± 0.71

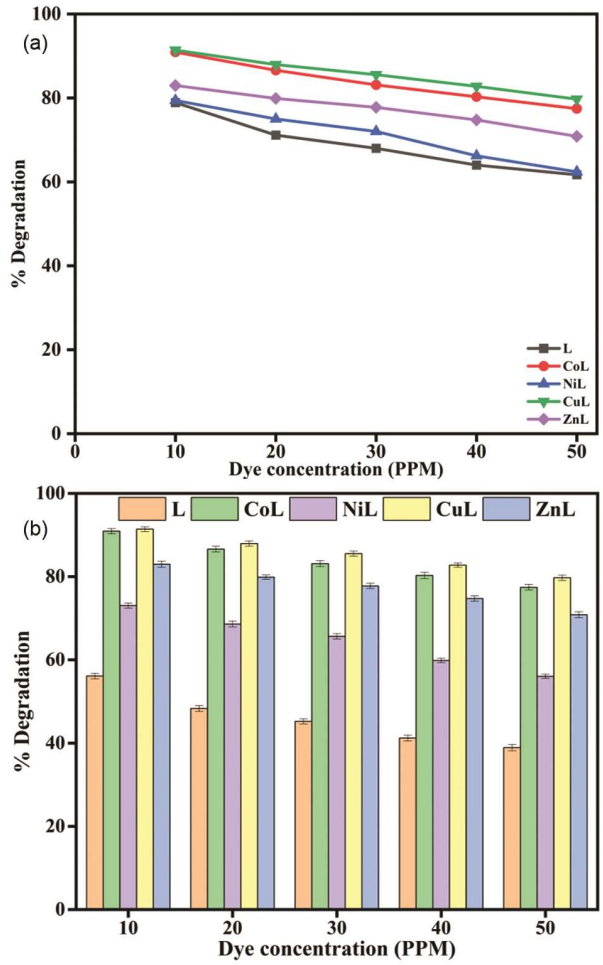

Fig. 17 — (a) Degradation of MB at initial concentration of dye at room temperature; and (b) Statistical representation of MB at initial concentration of dye at room temperature

Figure 17a & b illustrate the statistical data and degradation of MB at various initial dye concentrations (10-50 PPM), followed by UV irradiation for 20 min intervals with 50 mg/L of the bioactive ligand L and its metal complexes (CoL, NiL, CuL, ZnL). It has been noted that less degradation occurs at higher dye concentrations. This may be attributed to the increase in the adsorption of dye on catalyst particles with the increase in concentration. Hence, the catalyst surface is not reached by the UV light. At higher concentrations, the depth of penetration of the dye is also reduced[39].

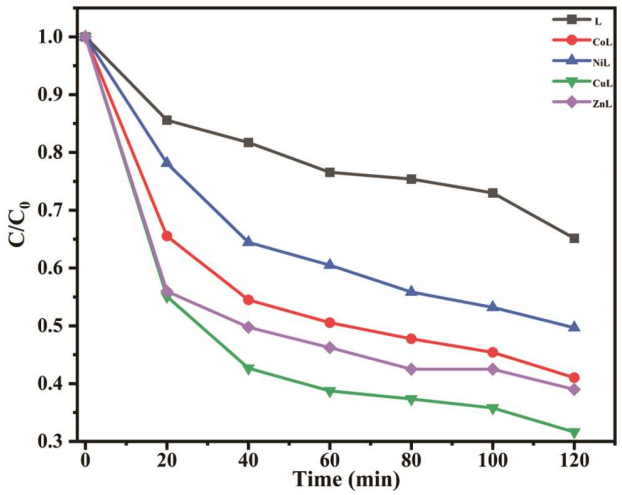

Fig. 18 — Degradation of MB at concentration 50 mg/L of the bioactive ligand L and its metal complexes at room temperature

Effect of catalytic dosages

The effect of various concentrations of the bioactive ligand L and its metal complexes (10 to 50 mg/L) on the rate of dye degradation of MB has been examined while keeping all other factors constant. It is clear that the rate of dye degradation (C/C_o *vs*. time) increased with the increase in the concentration of the bioactive ligand L and its metal complexes (CoL, NiL, CuL, ZnL). The highest degradation was observed at 50 mg/L of compounds used, while the lowest degradation was noted at 25 mg/L due to the availability of fewer active sites. When the concentration was increased to 50 mg/L, the dye degradation rate also increased, which could be attributed to the availability of a greater number of active sites (Fig. 18). Further increases in concentration (above 50 mg/L) did not result in significant degradation. Therefore, 50 mg/L of compounds has been considered optimal[40]. The plot of remaining concentrations (10, 20, 30 and 40 mg/L) were provided in supplementary data (Suppl. Fig. S4a-d).

Contact time

Adsorption of MB on the surface of the adsorbent (bioactive ligand L and its metal complexes), is a function of the contact time. This is corresponding to the time of adsorption, or the state of saturation of the adsorbent surface by the adsorbate (dye). Table 11 represents the effect of contact time with statistical data on the removal of MB using 50 mg/L of catalysts in aqueous solution (Fig 19a & b). The result show that the catalysis of decomposition of MB occurs. It was observed that, the efficiency of MB decolorization utilizing the individual adsorbent is quite different. However, for the Cu and Co metal complexes, the degradation was high (71.4%) as compared with others after 120 min irradiation under UV light[41].

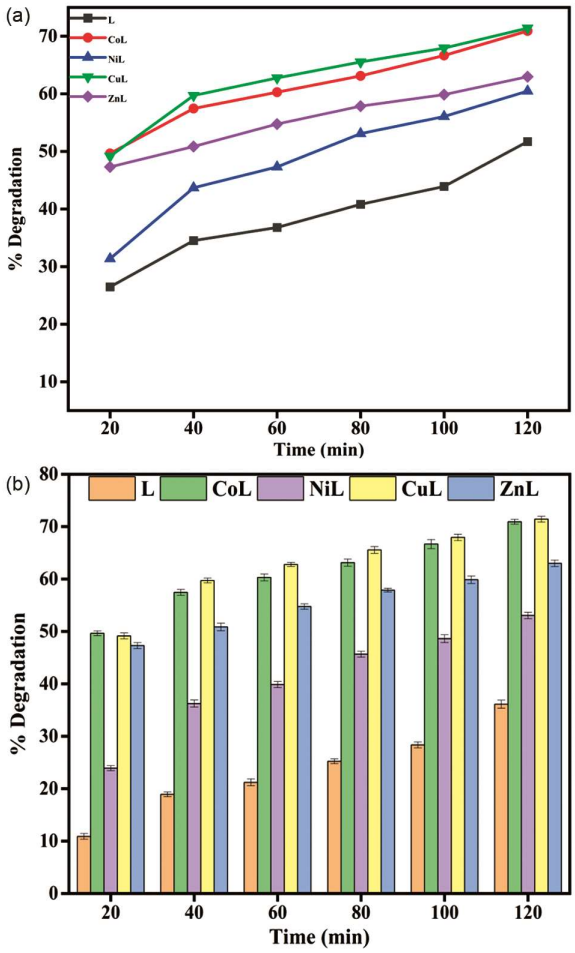

Fig. 19 — (a) Effect of contact time on the removal of MB using 50 mg/L of catalysts; (b) Statistical representation of contact time on the removal of MB using 50 mg/L of catalysts

Proposed mechanism for degradation of dye

Bioactive ligand L behaves as a bidentate ligand through N and O coordinating atoms. The UV irradiation helps to excitation of electron. A tentative mechanism proposed for the dye degradation in presence of bioactive ligand L and its metal complexes (CoL, NiL, CuL, ZnL) and possible reaction are represented in (Fig. 20). When excited species (*) captures an electron from water, becomes an active species ($^{\circ}$OH). Reduced metal complexes $[ML]^{-}$ will be immediately re-oxidized in the presence of O_2 for completing the regeneration of catalysts[42].

Kinetic study of dye degradation

Degradation of dye (MB) under UV irradiation follows pseudo first order kinetics. The expression Eq. (4)

$$ln\frac{C_0}{C} = k.t \quad \text{... (4)}$$

Where rate constant is represented by k, initial concentration of MB solution represented by C_0 and C is concentration of MB solution at the reaction time[43].

Figure 21 represented the linear plots with correlation coefficient (R^2) average value 0.962 for the bioactive ligand L and its metal complexes (CoL, NiL, CuL, ZnL). This is the evidence for the pseudo first order reaction; the reactants should be present in large amount, so the concentration of the reactant remains constant. Slight deviation from linearly plot indicates the insufficient amount of reactants.

Adsorption isotherm

The Langmuir, Freundlich, and Temkin equations are commonly employed as adsorption isotherm

Table 11 — Statistical representation of contact time

Time (min)	% Degradation				
	L	CoL	NiL	CuL	ZnL
20	10.891 ± 0.56	49.645 ± 0.45	23.913 ± 0.47	49.149 ± 0.56	47.304 ± 0.58
40	18.917 ± 0.45	57.446 ± 0.56	36.231 ± 0.67	59.716 ± 0.46	50.851 ± 0.74
60	21.210 ± 0.65	60.283 ± 0.65	39.855 ± 0.57	62.766 ± 0.37	54.752 ± 0.53
80	25.222 ± 0.46	63.12 ± 0.67	45.652 ± 0.57	65.532 ± 0.65	57.872 ± 0.37
100	28.343 ± 0.57	66.666 ± 0.87	48.62 ± 0.75	67.943 ± 0.61	59.858 ± 0.71
120	36.114 ± 0.76	70.921 ± 0.46	53.043 ± 0.63	71.418 ± 0.55	62.979 ± 0.61

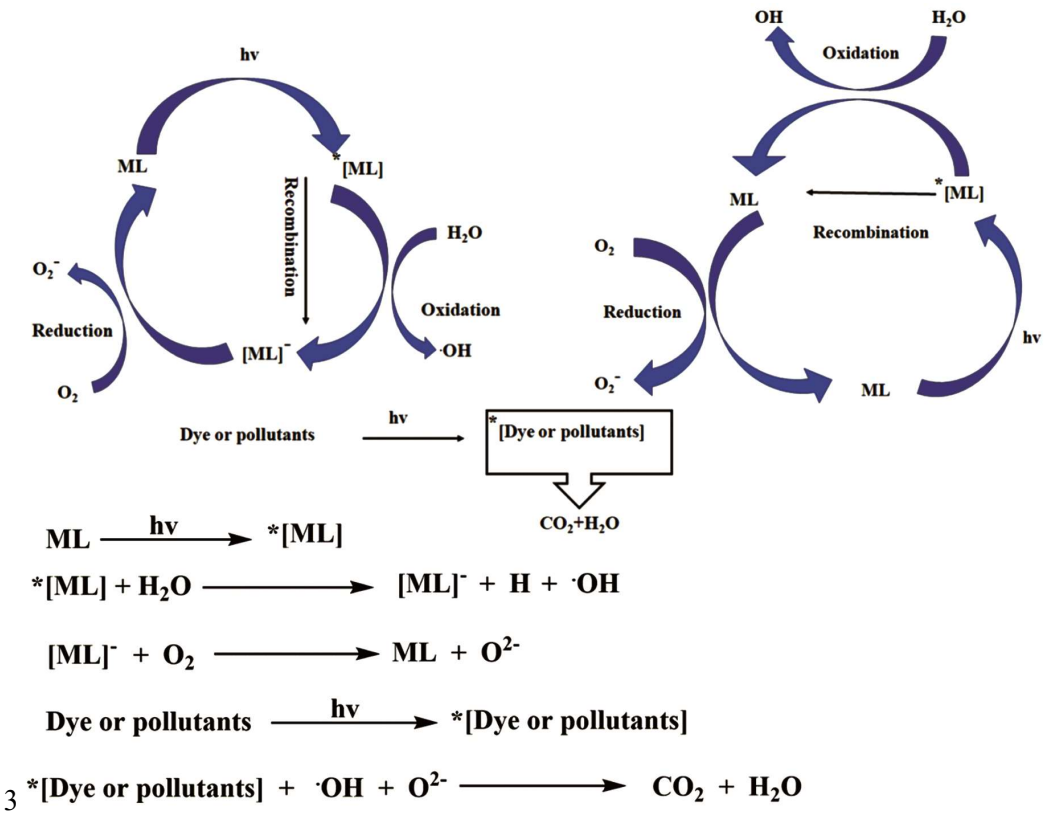

Fig. 20 — Proposed mechanism for degradation of dye and general reactions of degradation of dyes

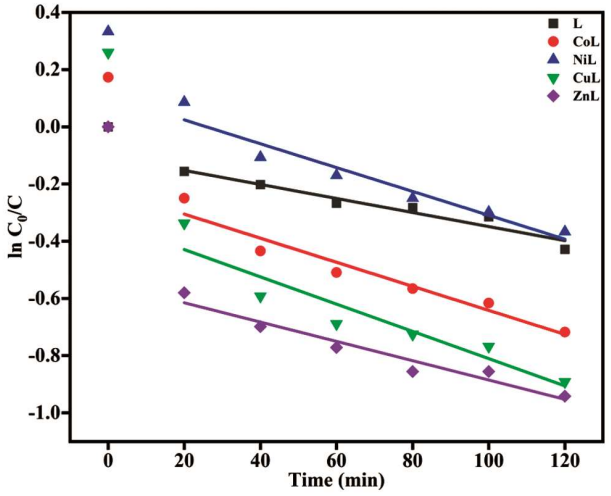

Fig. 21 — Pseudo first order kinetic of MB adsorption on L and its metal complexes

models to illustrate the interaction between adsorbents and adsorbates during the adsorption process. These isotherm equations are Eqs. (5-7) defined as follow:

$$\frac{1}{q_e} = \frac{1}{K_L q_{max}} \cdot \frac{1}{C_e} + \frac{1}{q_{max}} \quad \ldots (5)$$

$$Log\ q_e = Log\ K_F + \frac{1}{n}\ Log\ C_e \quad \ldots (6)$$

$$q_e = \frac{RT}{b_T} \ln A_T + \left(\frac{RT}{b_T}\right) \ln C_e \quad \ldots (7)$$

Here, C_e (mg L^{-1}) denotes the equilibrium concentration of adsorbate; q_e (mg g^{-1}) refers to the amount of adsorbate adsorbed per unit mass of adsorbent at equilibrium; q_m (mg g^{-1}) represents the maximum adsorption capacity. The constants K_L, K_F, and K_T correspond to the Langmuir, Freundlich, and Temkin isotherm models, respectively. Moreover, *n* indicates the adsorption intensity, *R* is the universal gas constant, *T* is the absolute temperature in Kelvin (K), and *b* is a constant associated with the heat of adsorption.

The adsorption isotherm curves for the adsorbate on bioactive ligand and its metal complexes are presented in (Fig. 22 & Suppl. Fig. S5 and S6), with the corresponding parameters listed in (Table 12). Based on the R^2 values from different isotherm models, the Langmuir model showed the best fit for the adsorption behavior of all the adsorbents. Specifically, the R^2 values were 0.74 for NiL, 0.55 for ZnL, and 0.53 for CuL. The K_L values for all the compounds were below 1, suggesting that the adsorption process were favorable and easily occurred. In contrast, the Freundlich and Temkin

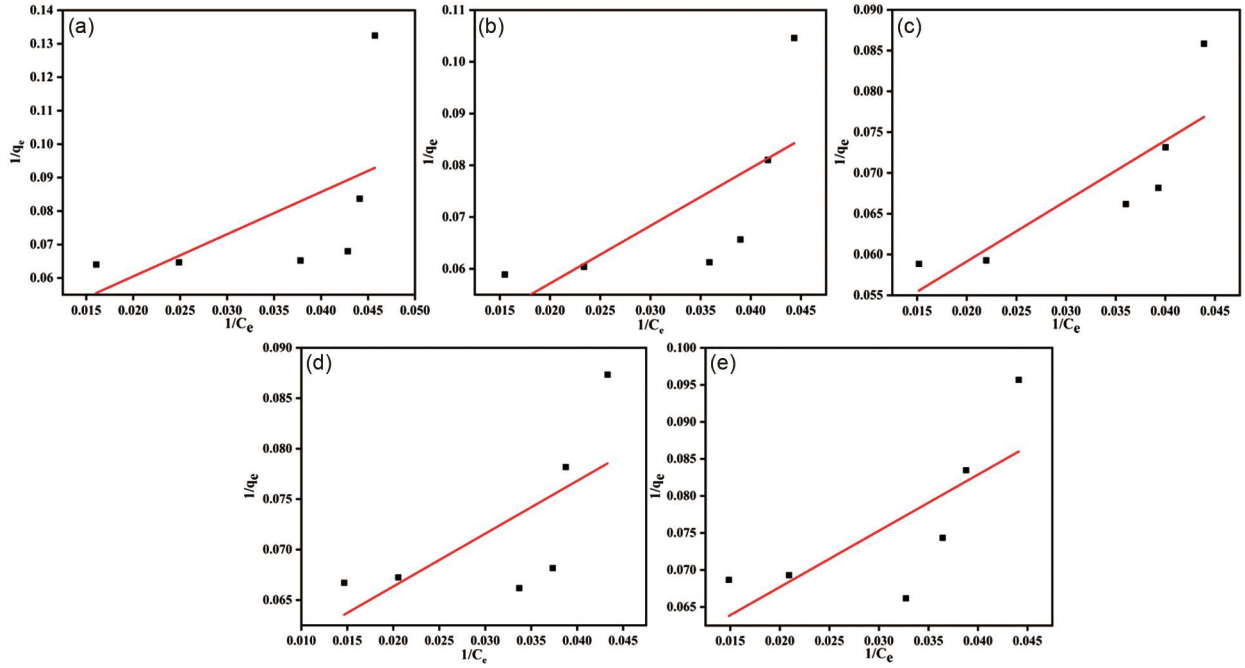

Fig. 22 — Langmuir adsorption isotherm for bioactive ligand and metal complexes

Table 12 — Parameters of Langmuir, Freundlich and Temkin adsorption isotherm models of bioactive ligand and metal complexes.

Samples	Langmuir			Freundlich			Temkin		
	q_{max} (mg/g)	K_L	R^2	K_F	1/n	R^2	b	K_T	R^2
L	28.38	0.02	0.25	3.63	0.37	0.22	4.46	0.03	0.24
CoL	28.66	0.03	0.47	3.94	0.36	0.41	5.02	0.01	0.47
NiL	22.56	0.05	0.74	5.61	0.27	0.70	4.08	0.44	0.72
CuL	17.89	0.10	0.53	7.78	0.16	0.52	2.19	229.4	0.53
ZnL	19.04	0.06	0.55	5.92	0.22	0.51	2.88	8.08	0.52

models had R^2 values below the Langmuir model for all adsorbents, indicating that they were less suitable for describing the adsorption behavior in this case (Suppl. Figs. S5 & S6)[44].

Conclusion

In this study, we successfully synthesized a bioactive Schiff base ligand, 2-chloro-6- ((2,5-dimethoxybenzylidene)amino)-4-nitrophenol (L), and its corresponding Co (II), Ni (II), Cu (II), and Zn (II) metal complexes. Spectral (IR, NMR, UV-Vis) and thermogravimetric analyses confirmed that the complexes adopt an octahedral geometry with slight distortions, and that the ligand acts as a bidentate donor. Powder XRD patterns supported their partially crystalline nature, while cyclic voltammetry revealed quasi-reversible, diffusion-controlled redox behavior. Density Functional Theory (DFT) studies provided deeper insight into the electronic structure, revealing global reactivity descriptors, HOMO-LUMO energy gaps, MEP maps, and optimized molecular geometries. Biologically, the metal complexes exhibited significant antimicrobial activity, with strong antifungal effects against *A. niger* and *F. oxysporum* (MIC 75%), and antibacterial effects against *E. coli* and *S. aureus* (MIC 50%). Antioxidant screening using the DPPH assay identified CuL as the most effective radical scavenger. In environmental assessments, all complexes demonstrated photocatalytic activity toward methylene blue degradation under UV light, with CuL again showing superior performance. The degradation followed pseudo-first-order kinetics and was optimal under basic pH conditions. Overall, the synthesized metal complexes display promising potential for dual applications in biomedical and environmental fields especially CuL, which stands out for both its bioactivity and photocatalytic efficiency in organic pollutant degradation.

Acknowledgement

The authors gratefully acknowledge the instrumentation facilities provided by the Institute Instrumentation Centre, IIT Roorkee; NIT Rourkela; and SAIF CSIR-CDRI, Lucknow. We thank the Department of Chemistry, Department of Botany, and the Center for Advanced Research (CAR), Dr. Harisingh Gour Vishwavidyalaya, Sagar, M.P., India, for their support. The authors also acknowledge UGC, New Delhi, India, for the Non-NET fellowship.

Conflict of interest

All authors declare no conflict of interest.

References

1 Saraswathi V, Agilan S, Muthukumarasamy N, Gupta VK, Suresh M, Peulakumari P & Velauthapillai D, Synthesis, crystal structure, Hirshfeld surface, nonlinear optical properties and computational studies of Schiff based (E)-N'-(2, 4-dimethoxybenzylidene) benzohydrazide single crystals for optoelectronic applications. *Opt Quantum Electron*, 54 (2022) 758.

2 Paul S & Barman P, NNO donor Schiff base metal complexes: Enzyme mimicking, DNA binding and biological insights. *J Mol Struct*, 1311 (2024) 138469.

3 Aljohani FS, Omran OA, Ahmed EA, Al-Farraj ES, Elkady EF, Alharbi A, Nashwa M El-Metwaly, Ibrahim OB & Abu-Dief AM, Design, structural inspection of new bis (1H-benzo [d] imidazol-2-yl) methanone complexes: biomedical applications and theoretical implementations via DFT and docking approaches. *Inorg Chem Commun*, 148 (2023) 110331.

4 Al-Shamry AA, Khalaf MM., El-Lateef HMA, Yousef TA, Mohamed GG, El-Deen KMK, Mohamed GG & Abu-Dief AM, Development of new azomethine metal chelates derived from isatin: DFT and Pharmaceutical Studies. *Mater,* 16 (2022) 83.

5 Abu-Dief AM, Alotaibi NH, Al-Farraj ES, Qasem HA, Alzahrani S, Mahfouz MK & Abdou A, Fabrication, structural elucidation, theoretical, TD-DFT, vibrational calculation and molecular docking studies of some novel adenine imine chelates for biomedical applications. *J Mol Liq*, 365 (2022) 119961.

6 Abu-Dief AM, El-Khatib RM, Aljohani FS, Al-Abdulkarim HA, Alzahrani S, El-Sarrag G & Ismael M, Synthesis, structural elucidation, DFT calculation, biological studies and DNA interaction of some aryl hydrazone Cr3+, Fe3+, and Cu2+ chelates. *Compu Biol Chem*, 97 (2022) 107643.

7 Nayak PA, Naik HB, Viswanath R & Kirthan BR, Green light emitting fluorescent [Zn (II) (Schiff base)] complexes as electroluminescent material in organic light emitting diodes. *J Phys Chem Sol*, 159 (2021) 110288.

8 Huang S, Zheng L, Zheng S, Guo H & Yang F, First fluorescence sensor for hydrazine ion: An effective "turn-on" detection based on thiophene-cyanodistyrene Schiff-base. *J Photochem Photobiol A Chem*, 427 (2022) 113851.

9 Salih NS, Yahya WI, Al-Labban HMY & Aljanaby AAJ, Schiff bases compounds prepared from Phenyl hydrazine as a starting material were Synthesized, Characterized, and their Biological activity was investigated. *Res J Pharm Technol*, 15 (2022) 3595.

10 Chen Y, Mi Y, Li Q, Dong F & Guo Z, Synthesis of Schiff bases modified inulin derivatives for potential antifungal and antioxidant applications. *Int J Biol Macromol*, 143 (2020) 714-723.

11 Abu-Dief AM, El-Metwaly NM, Alzahrani SO, Bawazeer AM, Shaaban S & Adam MSS, Targeting ctDNA binding and elaborated *in vitro* assessments concerning novel Schiff base complexes: Synthesis, characterization, DFT and detailed *in silico* confirmation. *J Mol Liq*, 322 (2021) 114977.

12 Kaswan P, Chalcogenated Schiff base ligands utilized for metal ion detection. *Inorg Chem Acta*, 556 (2023) 121610.

13 Adeleke AA, Zamisa SJ, Islam MS, Olofinsan K, Salau VF, Mocktar C & Omondi B, Quinoline functionalized schiff base silver (I) complexes: interactions with biomolecules and *in vitro* cytotoxicity, antioxidant and antimicrobial activities. *Molecules,* 26 (2021) 1205.

14 Devi J, Kumar S, Kumar B, Asija S & Kumar A, Synthesis, structural analysis, *in vitro* antioxidant, antimicrobial activity and molecular docking studies of transition metal complexes derived from Schiff base ligands of 4- (benzyloxy)-2-hydroxybenzaldehyde. *Res Chem Intermed*, 48 (2022) 1541.

15 Gu YX, Chen LS & Nie L, Determination of 11 Kinds of Hair Dyes in Hair-Dyeing Products by Liquid Chromatography–Tandem Mass Spectrometry. *J Chromatogr Sci*, 62 (2023) 499.

16 Nawaz SS, Manjunatha KB, Ranganatha S, Supriya S, Ranjan P, Chakraborty T & Ramakrishna D, Nickel curcumin complexes: Physico chemical studies and nonlinear optical activity. *Opl Mater*, 136 (2023) 113450.

17 Djouama H, Djouama R, MacLeod-Carey D & Nafti N, Geometry optimization and UV/Vis spectra of organometallic chalcones functionalized with a benzo-15-crown-5 fragment: A DFT/TD-DFT investigation. *Inorg Chim Acta*, 561 (2024) 121866.

18 Khatri S, Khatri D, Lather V, Singh Y, Kumari P, Khatkar SP, Taxak VB & Kumar R, Exploration of Optical and Radiative Properties of Fluorinated β-keto Carboxylate Tb^{3+} Complexes Emanating Cool Green Light. *J Fluoresc*, 5 (2023) 1861.

19 Gogoi HP, Verma AK, Gogoi M, Goswami N & Barman P, Design, synthesis, and characterization of M (II)-Schiff base complexes containing 3, 5-di-tert-butyl salicylaldehyde: DNA binding/cleavage, DPPH radical scavenging activity, cytotoxic activity, and catalytic activity investigation. *Inorg Chem Commun*, 165 (2024) 112462.

20 Sultana S, Akramullazi A, Hossen MF, Asraf MA & Kudrat-E-Zahan M, Transition metal (II) complexes of 2- (2, 5-dimethoxy-benzylidene) hydrazine-1-carbothioamide: synthesis, characterization and their biological evaluation. *Mediterr J Chem*, 2 (2024) 122.

21 Slassi S, Aarjane M & Amine A, Synthesis, spectroscopic characterization (FT-IR, NMR, UV-Vis), DFT study, antibacterial and antioxidant *in vitro* investigations of 4, 6-bis ((E)-1- ((3- (1H-imidazol-1-yl) propyl) imino) ethyl) benzene-1, 3-diol. *J Mol Struct*, 1255 (2022) 132457.

22 Atzin-Macedo CM, Pastor-Ramírez C, González-Peláez R, Pérez-Flores FJ, Hernández-Anzaldo S, Vazquez-Lima H & Reyes-Ortega Y, Tautomeric Study of Schiff Bases Derived from o-Dihydroxybenzaldehyde by UV-Vis, IR, 1H NMR, 13C NMR Spectroscopy and Computational Modeling. *Chem Select*, 36 (2020) 11120.

23 Ekowo LC, Eze SI, Ezeorah JC, Groutso T, Atiga S, Lane JR, Okafor S, Akpomie KG & Okparaeke OC, Synthesis, structure, Hirshfeld surface, DFT and *in silico* studies of 4-[(E)- (2, 5-dimethoxybenzylidene) amino]-1, 5-dimethyl-2-phenyl-1, 2-dihydro-3H-pyrazol-3-one (DMAP) and its metal complexes. *J Mol Struct*, 1210 (2020) 127994.

24 Buldurun K, Turan N, Bursal E, Aras A, Mantarcı A, Çolak N, Türkan F & Gülçin I, Synthesis, characterization, powder X-ray diffraction analysis, thermal stability, antioxidant properties and enzyme inhibitions of M (II)-Schiff base ligand complexes. *J Biomol Struct Dyn*, 39 no. 17 (2021) 6480-6487.

25 Amereih S, Daraghmeh A, Warad I & Al-Nuri M, Synthesis, Characterization and Evaluation of Biological Activity of Sulfonylhydrazide-Schiff Base" (E)-N'- (2, 5-dimethoxybenzalidene) naphthalene-2-sulfonohydrazid. *Pal Tech Univ Res J,* (2020) 1.

26 El-Boraey HA, El-Gammal OA & Abdel Sattar NG, Impact of gamma-ray irradiation on some aryl-amide-bridged Schiff-base complexes: spectral, TGA, XRD, and antioxidant properties. *J Radioanal Nucl Chem*, 323 (2020) 241.

27 Kargar H, Behjatmanesh-Ardakani R, Fallah-Mehrjardi M, Torabi V, Munawar KS, Ashfaq M & Tahir MN, Ultrasound-based synthesis, SC-XRD, NMR, DFT, HSA of new Schiff bases derived from 2-aminopyridine: Experimental and theoretical studies. *J Mol Struct*, 1233 (2021) 130105.

28 Paul S & Barman P, Exploring diaminomaleonitrile-derived Schiff base ligand and its complexes: Synthesis, characterization, computational insights, biological assessment, and molecular docking. *J Mol Struct*, 1296 (2024) 136941.

29 Fathi AM, Mandour HS & Hassane Anouar E, Characteristics of multidentate Schiff base ligand and its complexes using cyclic voltammetry, fluorescence, antimicrobial behavior and DFT-calculations. *J Mol Struct*, 1224 (2021) 129263.

30 Benabid W, Ouari K, Bendia S, Bourzami R & Ait Ali M, Crystal structure, spectroscopic studies, DFT calculations, cyclic voltammetry and biological activity of a copper (II) Schiff base complex. *J Mol Struct*, 1203 (2020) 127313.

31 Bishoyi AK, Mahapatra M, Sahoo CR, Paidesetty SK & Padhy RN, Design, molecular docking and antimicrobial assessment of newly synthesized p-cuminal-sulfonamide Schiff base derivatives. *J Mol Struct*, 1250 (2022) 131824.

32 Joshi KA, Singh K, Mishra H & Pokharia S, Triorganotin (IV) complexes of Schiff base derived from 1, 2, 4-triazole moiety: Synthesis, spectroscopic investigation, DFT studies, antifungal activity and molecular docking studies. *J Mol Struct*, 1206 (2020) 127639.

33 Xu Y, Shi Y, Lei F & Dai L, A novel and green cellulose-based Schiff base-Cu (II) complex and its excellent antibacterial activity. *Carbohydr Polym*, 230 (2020) 115671.

34 Kaya S, Erkan S & Karakaş D, Computational investigation of molecular structures, spectroscopic properties and antitumor-antibacterial activities of some Schiff bases. *Spectrochim Acta A Mol Biomol Spectrosc*, 244 (2021) 118829.

35 Al-Ahmary KM, Shafie A, Adnan Ashour AS, Alrashdi K, Babalghith AO, Alharthi SS & Sabei FY, Recent Advances in Calixarenes for the Detection of Metal Ions, Bioimaging Applications, and Anticancer Activities: A Comprehensive Review. *Crit Rev Anal Chem*, (2024) 1.

36 Ashour AA & Shafie A, Recent progress in cellulose derivatives and cellulose-based composites for bioimaging and anticancer applications. *Cellulose*, (2024) 1.

37 Gogoi HP & Barman P, Salophen type ONNO donor Schiff base complexes: synthesis, characterization, bioactivity, computational, and molecular docking investigation. *Inorg Chim Acta*, 556 (2023) 121668.

38 Varshney A & Mishra AP, Synthesis, spectral characterization, computational studies, antifungal, DNA interaction, antioxidant and fluorescence property of novel Schiff base ligand and its metal chelates. *Spectrochim Acta A Mol Biomol Spectrosc*, 297 (2023) 122765.

39 Gerasimova MA, Tomilin FN, Malyar EY, Varganov SA, Fedorov DG, Ovchinnikov SG & Slyusareva EA, Fluorescence and photoinduced proton transfer in the protolytic forms of fluorescein: Experimental and computational study. *Dyes Pigm*, 173 (2020) 107851.

40 Katouah HA, Facile synthesis of Co_3O_4 and ZnO nanoparticles by thermal decomposition of novel Co (II) and Zn (II) Schiff base complexes for studying their biological properties and photocatalytic degradation of crystal violet dye. *J Mol Struct*, 1241 (2021) 130676.

41 Ben SK, Gupta S, Harit AK, Raj KK & Chandra V, Enhanced photocatalytic degradation of Reactive Red 120 dye under solar light using BiPO4@ g-C_3N_4 nanocomposite photocatalyst. *Environ Sci Pollut Res*, 56 (2022) 84325.

42 Ben SK, Gupta S, Harit AK, Raj KK & Chandra V, Synthesis of g-C_3N_4, $Zn_3(PO4)_2$ and g-C_3N_4/Zn_3 $(PO_4)_2$ composites for application in photodegradation of crystal violet dye under solar light. *Chem Select*, 28 (2021) 7002.

43 Tichapondwa SM, Newman JP & Kubheka O, "Effect of TiO2 phase on the photocatalytic degradation of methylene blue dye. *Phys Chem Earth*, *Pt A/B/C*, 118 (2020) 102900.

44 Chen L, Li Z, Li W, Chen Z, Chen G, Yang W, Zhang X & Liu X, Investigation of adsorption kinetics and the isotherm mechanism of manganese by modified diatomite. *ACS Omega*, 25 (2021) 16402.